CHAPTER II

ANION AND AMINO ACID SENSORS

2.1 Introduction

In view of the importance of anions in various biological processes, medicine, and environment, the design of receptors for anion recognition has become an area of great interest.[38]

Imidazole is an important group in biological system [39, 40], 1,3-disubstiuented imidazole, namely imidazolium, is expected to be a good binding subunit for anions through cation-anion interactions and unconventional hydrogen bonds.[41] Moreover, Imidazolium salts, which interact with anions through formation of strong $(C\text{-}H)^{+}\cdots\cdots X^{-}$ ionic hydrogen bond, have also been used for anion recognition.

2.1.1 Literature review of Benzimidazolium derivatives

Khatri, V. K. and coworkers[42] designed and synthesized deoxychlolic acid-based cyclicbisimdazolium receptor **7** and **8** with *m*- and *p*-xylene as spacers. Upon addition of anion to receptor, it was expected that the C(2)-H proton of each imidazolium moiety is suggesting the complexation of the anion by $(C\text{-}H)^{+}$ hydrogen bonds. From NMR study, a Job Plot analysis also showed formation of 1:1 complex between these receptors and anion. The receptor with *m*-xylene shows a moderate selectivity for fluoride ion whereas the receptor with *p*-xylene exhibits highly affinity and selectivity towards the chloride ion.

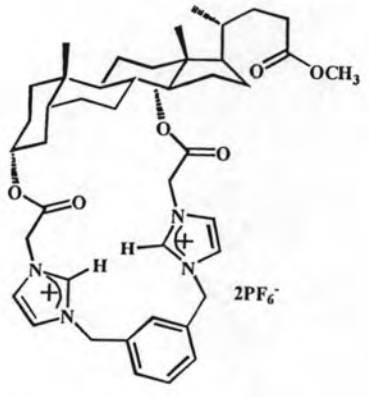

7

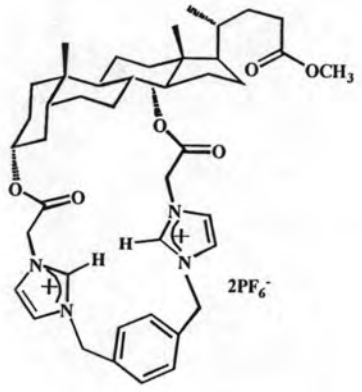

8

Yun, S. and coworker[43] reported on a new cavitand derivative bearing four imidazolium groups as a receptor **9** for anions. The tetrabutylammonium salts of various anions such as 1,3-adamantanedicarboxylate, adipate, terephthalate, 1,4-phenylenediacetate, succinate, acetate, Cl^-, Br^- and I^- were used for the binding studies. It was found that the cavitand displayed 1:1 binding with dicarboxylate except succinate. The case of succinate, acetate, Cl^-, Br^- showed 2:1 ratio with the host. From the association constants measured by ^{1}H-NMR experiment, they indicated that the length of the linker between two carboxylates as well as rigidity and flexibility of the guest are important effects on the binding of the cavitand. Moreover, the binding of the cavitand with these anions decreased in a more polar solvent due to the strong interaction of a polar solvent and the cationic imidazolium receptor.[44]

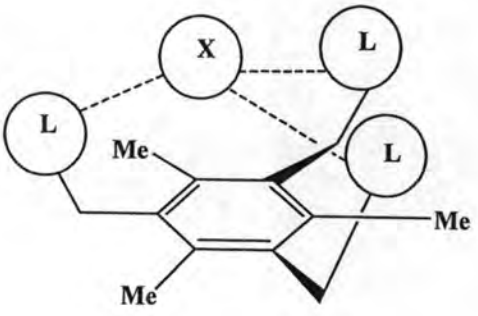

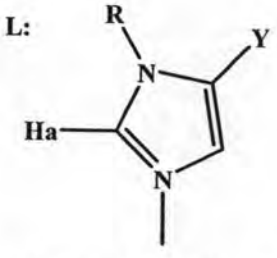

9 R= n-Bu, Y=H, Z = CH_2

Singh, N. J. and coworkers[45] reported four new fluorescent anion receptors including **10** (open form), **11**, **12** and **13** (closed form) bearing two imidazolium groups at the 2,3-positions of quinoxaline. From fluorescence studies of **10-13**, in the presence of anions, the spectra showed anion induced excimer formation at 430 nm in the attribution of the intermolecular π-π stacking between two antiparallel quinoxaline rings. On the other hand, **11** was ruled out of the excimer formation because the distance between the center of mass of two quinoxaline rings is not suitable for formation.[46] The deprotonation of **10** and **12** in the presence of $HP_2O_7^{3-}$ and acetate made the appearence of the fluorescent peak at 500 nm corresponding to charge-transfer phenomena from quinoxaline to deprotonated imidazolium moitety. The ^{1}H-NMR binding studies of F^- or acetate for **11-13** showed the disappearence of the corresponding $(C\text{-}H)^+$ peak at 1:1 equivalent of anion and host in acetonitrile.

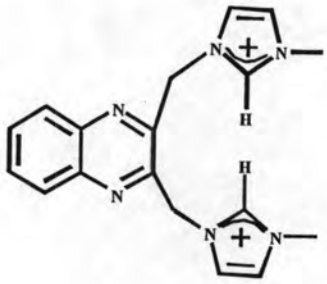

10

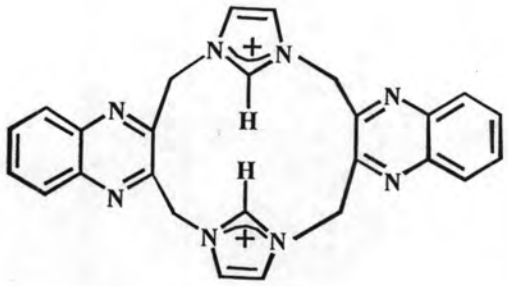

11

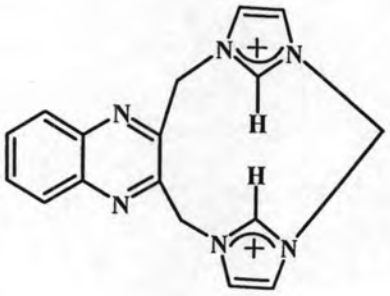

12

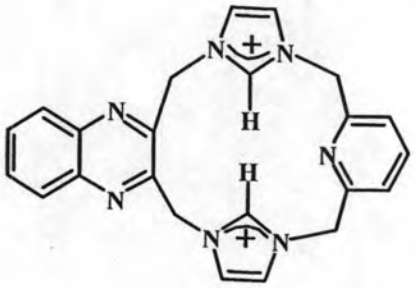

13

Ihm, H. and coworkers[47] synthesized the receptor **14, 15** and **16**. Host **14** contained imidazole as anion binding site which was obtained by adding a nitro group to the imidazolum sidearm and present enhanced anion affinity compared to those of hosts **15** and **16**. Anion binding properties of hosts **14-16** were investigated by ^{1}H NMR technique. Upon addition of chloride anion to host **14**, C(2) proton of imidazolum moiety was shifted to downfield under CH hydrogen bond. It is indicatived of a higher selectivity for chloride over bromide and iodide. The selectivity is in order of Cl^->Br^->I^-. The case of host **15** without nitro group attached on imidazolium unit showed a much smaller selectivity with halide anions compared to host **14** as a consequence of stronger $(C\text{-}H)^+$---X^- hydrogen bonds by more electron-deficient imidazolium moiety of host **14**. The binding property of host **16** containing *n*-butyl groups in imidazolium moieties suggested that *N*-substituents in imidazolium moieties did not directly affect on the complexation of anion.

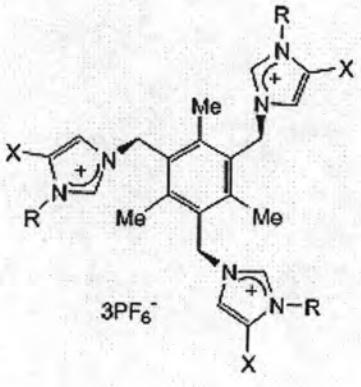

14 R = Me, X = NO_2

15 R = Me, X = H

16 R = *n*-Bu, X = H

Yoon, J. coworkers[48] have studied the benzene –based tripodal imidazolium receptors utilizing the strong $(C\text{-}H)^{+}\text{---}X^{-}$ charged hydrogen bonding between imidazolium moieties. They have recently reported an anthracene derivative bearing two imidazolium on its 1,8-position but this receptor is flexible. Interestingly, the proton on carbon which is a linking between anthracence and imidazole unit are able to bind with anion *via* hydrogen bonding interaction. Therefore, they designed a molecular system where the receptor sites has been utilized with help of two rigid frames at both left and right sides to avoid the interaction between the hydrogen of the connecting CH_2 and anions. From ^1H NMR studies, upon addition of 3 equiv. of Cl^- and Br^- to host **17**, the spectrum displayed a large downfield shifts of C(2) proton of imidazolium moieties. It is suggesting **17**-anion complexation undergoes CH^+-anion charged hydrogen bonds. Concerning to the fluorescence titration of **17** with addition of various anions, the association constant for $H_2PO_4^-$, F^-, Cl^-, and Br^- are examined to be >1300000, 340000, 2000 and 780 M^{-1}, respectively. The selectivity is in trends $H_2PO_4^->Cl^->Br^-$. These binding phenomena can be monitored *via* fluorescence quenching effects.

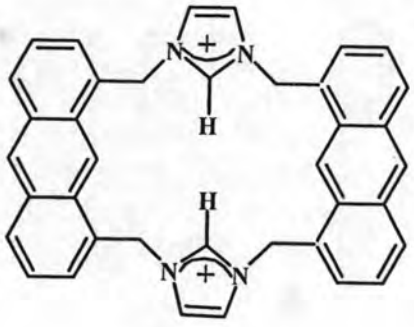

17

2.1.2 Target Molecules

The literature review showed that the benzimidazolium derivative receptors are to be a good subunit for anion through the $(C\text{-}H)^{+}\cdots\cdots X^{-}$ ionic hydrogen bond. Moreover, the anthraquinone unit is able to bind the guest such as anions using cyclic voltammetry for detecting interaction behavior. Therefore, we have designed the benzimidazolium derivative receptors bearing anthraquinone for anions and amino acids. The benzimidazolium derivative receptors $\mathbf{L^1H}$, $\mathbf{L^2H}$ and $\mathbf{L^3H}$ were shown in figure 2.1.

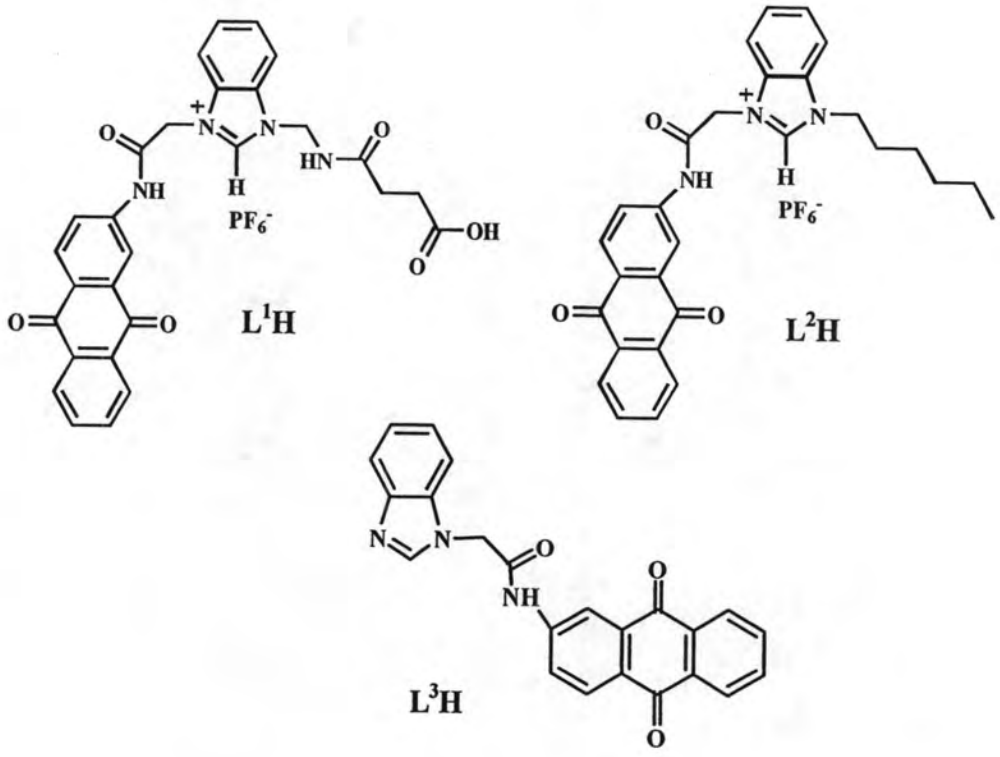

Figure 2.1 Target molecules

2.2 Experimental section

2.2.1 Synthesis part

2.2.1.1 General procedure

2.2.1.1.1 Analytical instruments

Nuclear magnetic resonance (NMR) spectra were recorded in DMSO-d_6, $CDCl_3$ or CD_3CN on Variance 400 MHz spectrometer. Electrospray mass specta were determined on a Micromass Platform quadupole mass analyser with an electrospray ion source using acetonitrile as solvent. All melting points were obtained on an Electrothermal 9100 apparatus and uncorrected. Infrared spectra were carried out on a Nicolet Impact 410 FTIR spectrometer at room temperature with the potassium bromide (KBr) disk method. The sample was scanned over a range of 500-4000 cm^{-1} at resolution of 16 cm^{-1} and the number of scan was 32. The measurement was controlled by Omnic software. Elemental analyses were carried out on a Perkin-Elmer CHON/S analyzer (PE

2400 series II) by ignition combustion gas chromatography separated by frontal analyses and quantitatively detected by thermal conductivity detector. Absorption spectra were measured by a Varian Cary 50 UV-Vis spectrophotometer. Cyclic voltammetry and square wave voltammetry were performed using an AUTOLAB PGSTAT 100 potentiostat.

2.1.1.1.2 Materials for synthesis

Unless otherwise specified, the solvents and all materials were reagent grades without further purification prior to use. Commercial grade solvents such as acetone, dichloromethane, hexane, methanol and ethyl acetate were purified by distillation before used. Acetonitrile, dimethylformamide and dichloromethane for set up the reaction were dried over calcium hydride and THF was dried over benzoquinone and sodium and freshly distilled under nitrogen atmosphere prior to use. All guests as salts and ligands were dried in *vacuo* prior to use. 1-*N*-(propanicaminomethyl)-*N*-chloroethylene amidoanthraquinone benzimidazole, $\mathbf{L^1H}$, 1-*N*-(propanicamino methyl)-*N*-hexyl benzimidazole, $\mathbf{L^2H}$ and methyleneamidoanhraquinone benzimidazole, $\mathbf{L^3H}$ were prepared and characterized by ^{1}H NMR spectroscopy, mass spectroscopy, FT-IR technique and elemental analysis.

2.2.1.2 Synthesis of benzimidazolium derivatives

2.2.1.2.1 Preparation of 1-*N*-(*N*-methyl-phthatimide)benzimidazole (1a)

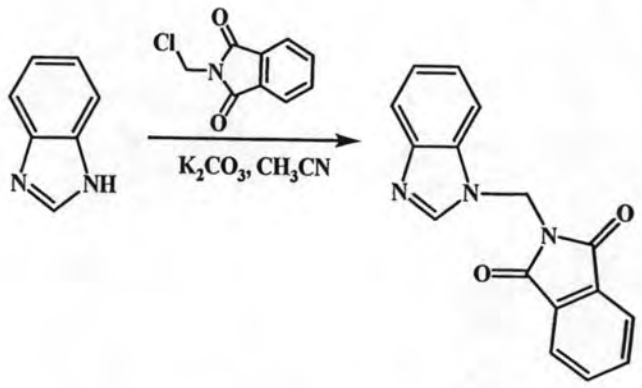

1a

A solution of benzimidazole (1.50 g, 12.70 mmol) and potassium carbonate (2.63 g, 19.10 mmol) was slowly stirred in 70 mL acetonitrile and added with a solution of *N*-(chloromethyl)phthatimide (3.72 g, 19.1 mmol) in acetonitrile. The reaction mixture was heated at reflux for 24 hours under nitrogen atmosphere. After evaporation in *vacuo*, the residue was dissolved in dichloromethane and washed with water (3 * 50 mL). The organic layer was dried over anhydrous sodium sulfate and concentrated under reduced pressure. The desired product was purified by column chromatography (SiO_2) using ethylacetate as eluent to yield the white solid (0.79 g, 76% yield).

Characterization data for 1a

^{1}H-NMR (400 MHz), $CDCl_3$): δ (ppm)

δ 8.33 (s, 1H, -NC*H*N-), 7.91 (m, 3H, -ArH-), 7.79(m, 3H, -ArH-), 7.35(m, 2H, -ArH-), 6.06 (m, 2H, -CH_2-).

ESI –TOF mass spectrun : $C_{16}H_{11}N_3O_2$ = 277.04 ([M+H^+]) m/z.

2.2.1.2.2 Preparation of 1-*N*-(*N*-methyl-amino)benzimidazole (2a)

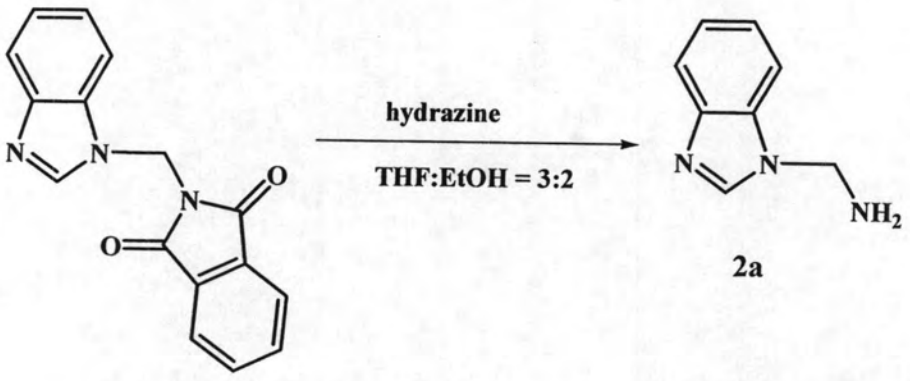

2a

To a solution of **1** (1.00 g, 3.60 mmol), hydrazine (0.87 mL, 18.10 mmol) was added in THF:EtOH = 3:2. The mixture was stirred for further 3 hours under nitrogen atmosphere. Then, the mixture solution was evaporated in *vacuo*. The residue was purified on a column chromatography (SiO_2) using 10% yield methanol/dichloromethane as eluent to obtain the desired product **2a** as a white solid (0.69 g, 76% yield).

Characterization data for 2a

^{1}H-NMR (400 MHz, $CDCl_3$): δ (ppm)

δ 8.06 (s, 1H, -NC*H*N-), 7.61 (m, 2H,- Ar*H*-), 7.23 (m, 2H, -Ar*H*-), 4.90 (m, 2H, -CH_2-).

2.2.1.2.3 Preparation of 1-*N*-(propanicaminomethyl)benzimidazole (3a)

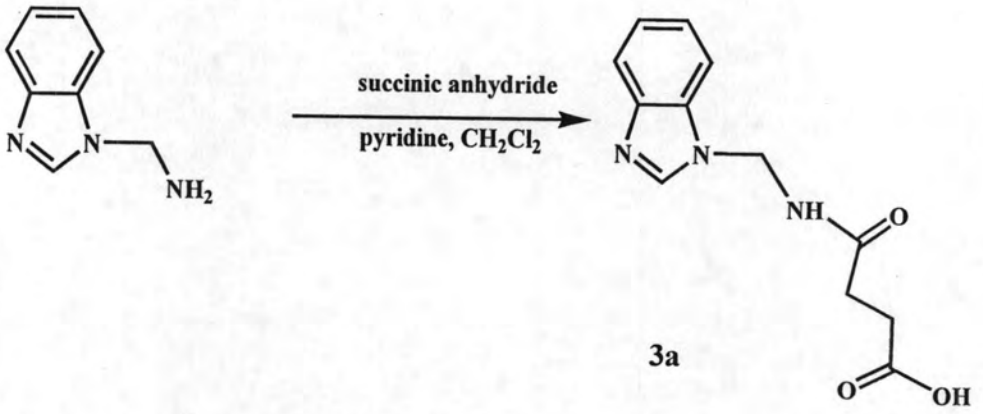

3a

A mixture of succinic anhydride (0.81 g, 8.20 mmol) and pyridine (0.65 mL, 8.20 mmol) was stirred in 40 mL dichloromethane for a while and then the solution of **2a** in dichloromethane was slowly added into the succinic solution and left stirring for 24 hours under nitrogen atmosphere. A white precipitate was observed in reaction and was acidified to pH 2 using glacial acetic acid. The adjusted solution was filtered to afford a white solid of **3a** (0.83 g, 90% yield).

Characterization data for 3a

^{1}H-NMR (400MHz, DMSO-d_6): δ (ppm)

δ 12.28 (broad, 1H, -COO*H*), 8.22 (s, 1H, -NC*H*N-), 7.61(m, 2H, - Ar*H*-), 7.20 (m, 2H, - Ar*H*-), 2.43(m, 6H, -CH_2-).

2.2.1.2.4 Preparation of Chloroethyleneamidoanthraquinone (4a)

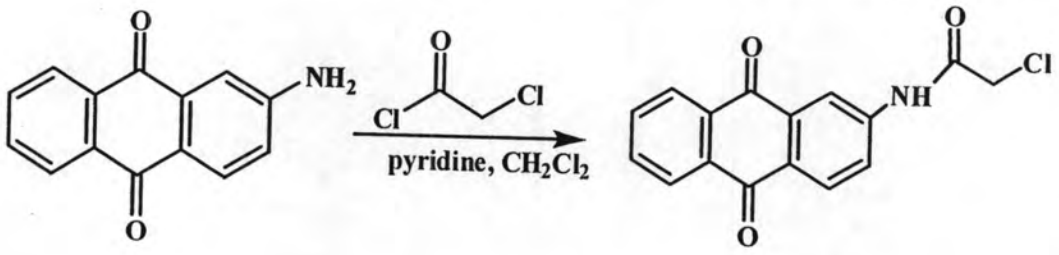

4a

A solution of aminoanthraquinone (1.00 g, 4.50 mmol) and pyridine (0.86 mL, 5.40 mmol) was stirred in 50 mL dichloromethane and cooled down to 0° C. After slowly adding the solution of chloroacetylchloride in dichloromethane, the brown precipitate appeared in the reaction. The mixture reaction was left stirring in 3M HCl in water for a while prior to extraction with water (3 * 50 mL). The organic layer was dried with sodium sulfate and evaporated in *vacuo* to obtain the brown solid which was crystallized by dichloromethane/hexane. The purified compound **4a** was yielded as a brown crystalline solid (0.68 g, 70% yield).

Characterization data for 4a

^{1}H-NMR (400MHz, $CDCl_3$): δ (ppm)

δ 8.64 (s, 1H, -N*H*-), 8.36 (m, 4H, -Ar*H*-), 8.26(s, 1H, -Ar*H*-), 7.85 (m, 2H, -Ar*H*-), 4.30 (s, 2H, -CH_2-).

ESI –TOF mass spectrun : $C_{16}H_{10}NO_3Cl$ = 299.03 ([M+H^+]) m/z.

2.2.1.2.5 Preparation of 1-*N*-(propanicaminomethyl)-*N*-Chloroethyleneamido anthraquinone benzimidazole (L^1H)

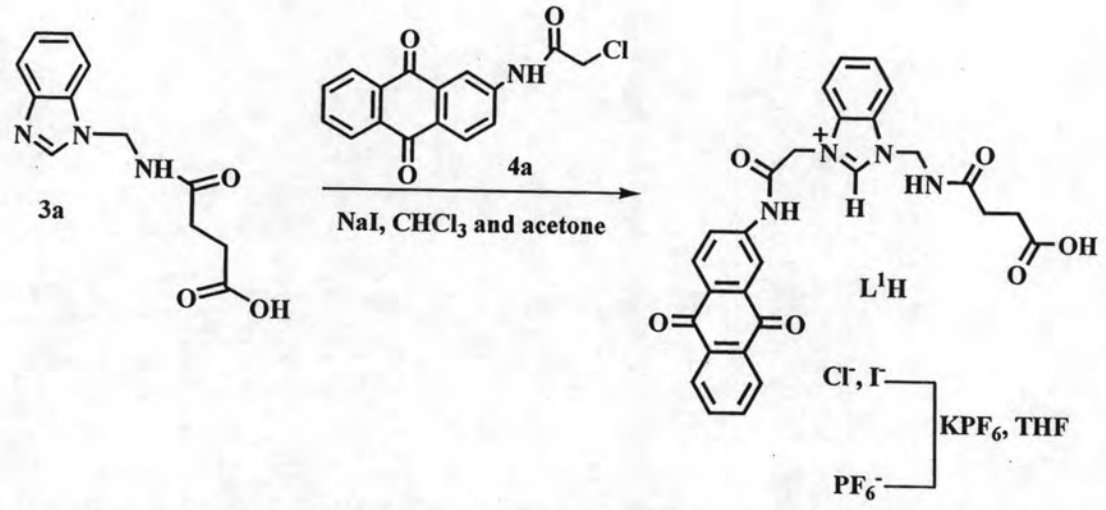

To a solution of **3a** (0.12 g, 0.50 mmol), **4a** (0.18 g, 0.60 mmol) was added and kept stirring in 15 mL of acetone/chloroform in the presence of a catalytic amount of sodium iodide. The precipitate was appeared from the mixture and recrystallized by the mixture solvents of dichloromethane/hexane to provide product $\mathbf{L^1Cl}$ (10% yield yield). Anion exchange of $\mathbf{L^1Cl}$ was accounted with KPF_6 in THF for 24 hours affording $\mathbf{L^1H}$ (0.80 g, 81% yield).

Characterization data for L^1H

^{1}H-NMR (400 MHz, DMSO-d_6): δ (ppm)

δ 11.22 (s, 1H, -N*H*-), 9.73 (s, 1H, -NC*H*N-), 9.06 (s, 1H, -N*H*-), 8.47 (s, 1H, -Ar*H*-), 8.21 (m, 3H, -Ar*H*-), 8.19 (m, 1H, -Ar*H*-), 7.91 (m, 2H, -Ar*H*-), 7.83 (m, 2H, -Ar*H*-), 7.47 (m, 2H, -Ar*H*-), 5.47 (s, 2H, -NCH_2CO-), 2.49 (m, 2H, -HOCH_2CO-), 2.48 (m, 2H, -CH_2-), 2.48 (m, 2H, -CH_2-).

^{13}C-NMR (400MHz, DMSO-d_6): δ (ppm)

δ: 27.96, 28.79, 48.40, 112.21, 116.03, 116.85, 126.74, 128.73, 134.29, 143.83.

ESI –TOF mass spectrum : $C_{32}H_{31}N_4O_7PF_6$ = 797.0 $(\mathbf{L^1H}+PF_6)^-$, 415.9 $(M+PF_6+Cl)^{2-}/2$

Elemental Analysis :

Anal Calcd for $C_{32}H_{31}N_4O_7PF_6$: C, 53.35; H, 3.64; N, 8.43.

Found: C, 52.86; H, 4.34; N, 8.41.

The compound is hygroscopic and is easy to absorb the moisture when exposed in air.

UV-Vis (DMSO) λ_{max} = 370 nm.

Melting point: 204-205 °C.

2.2.1.2.6 Preparation of 1-*N*-(*N*-hexyl)benzimidazole (5a)

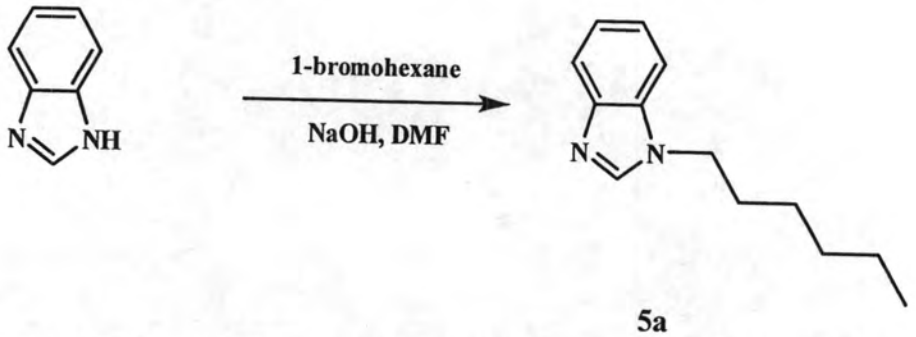

5a

To a stirred solution of benzimidazole (0.50 g, 4.20 mmol) and sodium hydroxide (0.17 g, 4.20 mol), a solution of hexylbromide (0.60 mL, 2.30 mmol) in dimethylformamide was slowly added and refluxed for 24 hours under nitrogen atmosphere. The reaction mixture was evaporated in *vacuo.* The residue was purified by column chromatography (SiO_2) using 50% yield ethylacetate/dichloromethane as eluent to afford compound **5a** as colorless liquid (0.48 g, 80% yield).

Characterization data for 5a

^{1}H-NMR (400 MHz, $CDCl_3$): δ (ppm)

δ 8.20 (s, 1H, -NC*H*N-), 7.57 (m, 2H, -Ar*H*-), 7.22 (m, 2H, -Ar*H*-), 4.20 (m, 2H, -NCH_2-), 1.75 (m, 2H, -CH_2-), 1.22 (m, 6H, -CH_2-), 0.79 (m, 3H, -CH_3).

2.2.1.2.7 Preparation of 1-*N*-(propanicaminomethyl)-*N*-hexyl benzimidazole (L^2H)

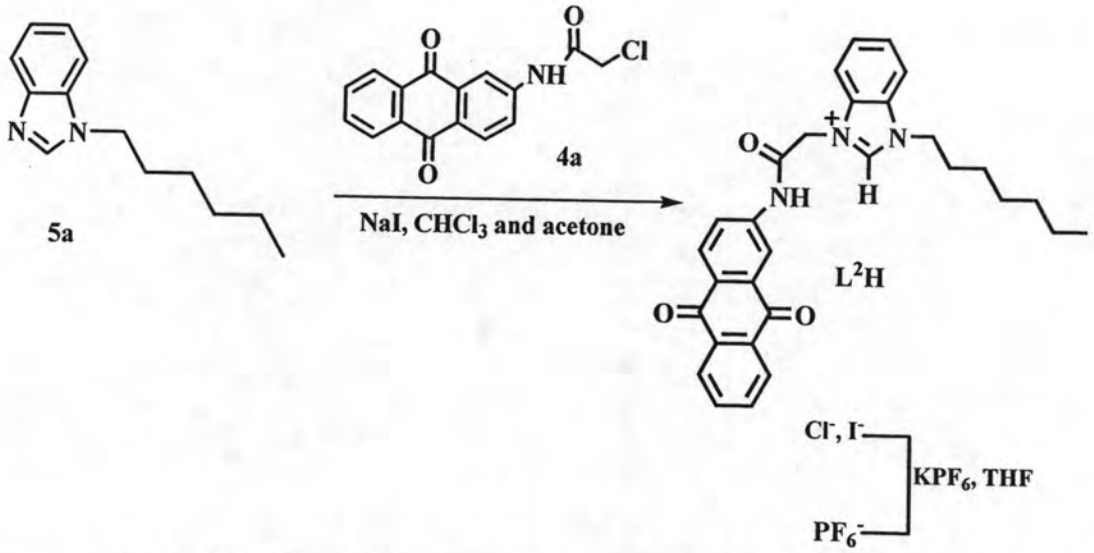

To a solution of **4a** (0.20 g, 1.00 mmol), **5a** (0.29 g, 1.00 mmol) was added and kept stirring in 15 mL of acetone/chloroform in the presence of a catalytic amount of sodium iodide. The precipitate was appeared from the mixture and recrystallized by the mixture solvents of dichloromethane/hexane to obtain product $\mathbf{L^2Cl}$ (10% yield yield). Anion exchange of $\mathbf{L^2Cl}$ was accounted with KPF_6 in THF for 24 hours affording $\mathbf{L^2H}$ (0.17 g, 81% yield).

Characterization data for L^2H

^{1}H-NMR (400MHz, DMSO-d_6): δ (ppm)

δ 11.30 (s, 1H, -N*H*-), 9.78 (s, 1H, -NC*H*N-), 8.48 (s, 1H, -Ar*H*-), 8.21 (m, 2H, -Ar*H*-), 8.15 (m, 2H, -Ar*H*-) , δ 8.08 (m, 2H, -Ar*H*-), 7.90 (m, 2H, -Ar*H*-), 7.70 (m, 2H, -Ar*H*-), 5.60 (s, 2H, -COCH_2N-), 4.58 (m, 2H, -NCH_2-), 1.91 (m, 2H, -CH_2-), 1.30 (m, 6H, -CH_2-), 0.83 (m, 3H, -CH_3).

^{13}C-NMR (400MHz, DMSO-d_6): δ (ppm)

δ: 14.17, 26.23, 29.26, 31.43, 48.01, 50.08, 125.01, 127.52, 127.81, 135.28, 143.84.

ESI –TOF mass spectrun : $C_{29}H_{28}N_3O_3PF_6$ = 466.21 ($\mathbf{L^2H^+}$).

Elemental Analysis:

Anal Calcd for $C_{29}H_{28}N_3O_3PF_6$: C, 56.96; H, 4.62; N, 6.87.

Found: C, 56.21; H, 4.87; N, 7.15.

The compound is hygroscopic and is easy to absorb the moisture when exposed in air.

UV-Vis (DMSO) λ_{max} = 368 nm.

m.p. = 305-306 ℃

2.2.1.2.8 Preparation of methyleneamidoanhraquinone benzimidazole(L^3H)

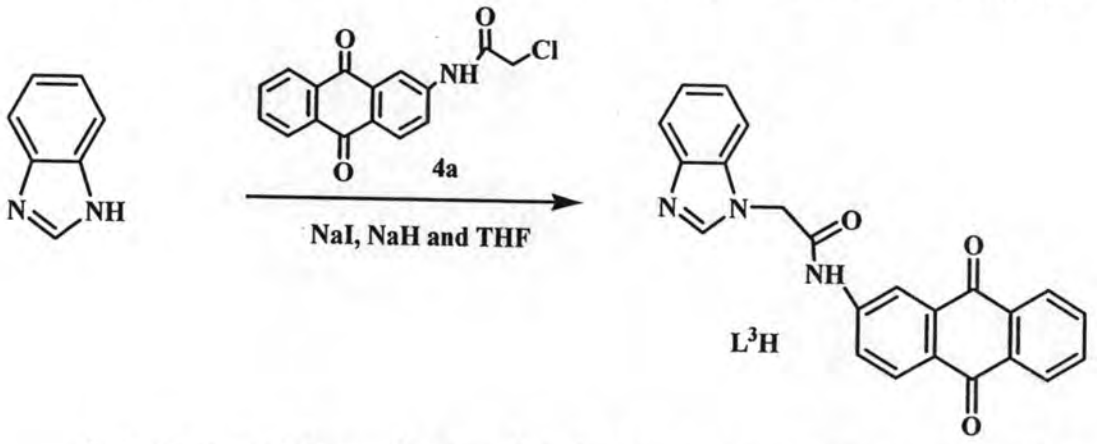

Into a two-necked round-bottomed flask, the mixture of benzimidazole (0.12 g, 0.50 mmol) and NaH (0.02 g, 0.50 mmol) as base were stirred at room temperature under N_2 atmosphere. A catalytic amount of sodium iodide and **4a** (0.18 g, 0.60 mmol) in 60 ml was transferred into the mixture reaction *via* cannula. The reaction was stirred for 24 hours under nitrogen atmosphere. Then, the mixture was evaporated in *vacuo*. The residue was purified by column chromatography (SiO_2) using 5:4:1 of dichloromethane : ethylacetate : methanol as eluent to afford compound **L^3H** as brown solid (0.09 g, 80% yield yield).

Characterization data for L^3H

^{1}H-NMR (400 MHz, DMSO-d_6): δ (ppm)

δ 11.131 (s, 1H, -CON*H*-), δ 8.449 (s, 1H, -NC*H*=N), δ 8.256 (s, 1H, -Ar*H*-), δ 8.200 (m, 3H, -Ar*H*-), δ 8.073 (d, 1H, -Ar*H*-), δ 7.892 (m, 2H, -Ar*H*-), δ 7.578 (d, 1H, -Ar*H*-(benzimidazole)), δ 7.559 (d, 1H, -Ar*H*-(benzimidazole)), δ 7.231 (m, 2H, -Ar*H*-(benzimidazole), δ 5.280 (s, 2H, -COCH_2-)

ESI –TOF mass spectrun : (ESI MS (ES+): $C_{23}H_{15}N_3O_3$= 381.764(100) [M+H^+]

Elemental Analysis :

Anal Calcd for $C_{23}H_{15}N_3O_3$: C, 72.43; H, 3.96; N, 11.02.

Found: C, 72.145; H, 3.97; N, 11.02.

2.2.2 Complexation studies

2.2.2.1 ^{1}H-NMR titration studies for complexation of ligand L^1H, L^2H and L^3H with various anions and amino acids

Typically, a 5 mM solution of a ligand ($3.0 * 10^{-3}$ mmol) in DMSO (0.6 mL) was prepared in a 5-mm NMR tube. An initial ^{1}H-NMR spectrum of the solution of the ligand was recorded. A 30 mM stock solution of guest molecules ($1.5 * 10^{-2}$ mmol) in DMSO (0.5 mL) was prepared in vial (shown in Table 2.1). The solution of a guest was added *via* microsyringe (10 μL portions) to the NMR tube. ^{1}H-NMR spectra were recorded after each addition.

Table 2.1 Volume and concentration of the tetrabutylammonium salts and the ligand used to prepare various tetrabutylammonium salts : ligand ratios.

Mole ratio guest : ligand	Volume of 0.1 M guest in DMSO	Concentration of guest molecule	Concentration of ligand
0.0 : 1.0	0	0	$3.33 * 10^{-3}$
0.2 : 1.0	0.004	$6.62 * 10^{-4}$	$3.33 * 10^{-3}$
0.4 : 1.0	0.008	$1.32 * 10^{-3}$	$3.29 * 10^{-3}$
0.6 : 1.0	0.012	$1.96 * 10^{-3}$	$3.2 * 10^{-3}$
0.8 : 1.0	0.016	$2.60 * 10^{-3}$	$3.24 * 10^{-3}$
1.0 : 1.0	0.020	$3.23 * 10^{-3}$	$3.22 * 10^{-3}$
1.2 : 1.0	0.024	$3.85 * 10^{-3}$	$3.20 * 10^{-3}$
1.4 : 1.0	0.028	$4.46 * 10^{-3}$	$3.18 * 10^{-3}$
1.6 : 1.0	0.032	$5.06 * 10^{-3}$	$3.16 * 10^{-3}$
1.8 : 1.0	0.036	$5.66 * 10^{-3}$	$3.14 * 10^{-3}$
2.0 : 1.0	0.040	$6.25 * 10^{-3}$	$3.12 * 10^{-3}$
2.5 : 1.0	0.050	$7.69 * 10^{-3}$	$3.07 * 10^{-3}$
3.0 : 1.0	0.060	$9.10 * 10^{-3}$	$3.03 * 10^{-3}$
3.5 : 1.0	0.070	$1.04 * 10^{-3}$	$2.98 * 10^{-3}$
4.0 : 1.0	0.080	$1.18 * 10^{-2}$	$2.94 * 10^{-3}$

2.2.2.2 UV-vis titration studies for complexes of ligand L^1H, L^2H and L^3H with anions and amino acids

Typically, a stock solution of 0.005 M solution of a ligand $\mathbf{L^1H}$ (5.0×10^{-6} mol) in 5 mL of DMSO (AR grade) was prepared in a volumetric flask. 0.75 mL of 0.005 M stock solution of ligand $\mathbf{L^1H}$ was pipetted into a 5 mL volumetric flask and the solution was adjusted to the marked volume with DMSO. 2 mL of $1.5 * 10^{-4}$ M stock solution of ligand $\mathbf{L^1H}$ was pipetted into a 1 cm pathlength quartz cuvette and absorption spectrum of $\mathbf{L^1H}$ was recorded from 300 to 600 nm at room temperature with a Varian Cary 50 UV-vis spectrophotometer. A solution of a guest in DMSO was prepared in a 10 mL volumetric flask (shown in Table 2.2). The solution of a guest was added directly to the cuvette by microburette and stirred for 30 second and absorption spectra of solution was recorded after each addition until absorbance of a new peak at 370 nm was constant.

Table 2.2 Volume and concentration of the tetrabutylammonium salts and the ligand used to prepare various tetrabutylammonium salts : ligand ratios

Moleratio guest : ligand	Volume of 4 mM guest in DMSO	Concentration of guest molecule	Concentration of ligand
0.66 : 1.0	0.05	$4.17 * 10^{-5}$	$1.46 * 10^{-4}$
1.32 : 1.0	0.10	$8.14 * 10^{-5}$	$1.42 * 10^{-4}$
1.98 : 1.0	0.15	$1.19 * 10^{-4}$	$1.39 * 10^{-4}$
2.64 : 1.0	0.20	$1.55 * 10^{-4}$	$1.36 * 10^{-4}$
3.30 : 1.0	0.25	$1.90 * 10^{-4}$	$1.33 * 10^{-4}$
3.96 : 1.0	0.30	$2.23 * 10^{-4}$	$1.30 * 10^{-4}$
4.62 : 1.0	0.35	$2.54 * 10^{-4}$	$1.27 * 10^{-4}$
5.28 : 1.0	0.40	$2.85 * 10^{-4}$	$1.25 * 10^{-4}$
5.94 : 1.0	0.45	$3.14 * 10^{-4}$	$1.22 * 10^{-4}$
6.60 : 1.0	0.50	$3.42 * 10^{-4}$	$1.20 * 10^{-4}$
7.66 : 1.0	0.58	$3.84 * 10^{-4}$	$1.16 * 10^{-4}$
8.72 : 1.0	0.66	$4.24 * 10^{-4}$	$1.12 * 10^{-4}$
9.79 : 1.0	0.74	$4.61 * 10^{-4}$	$1.09 * 10^{-4}$
10.85 : 1.0	0.82	$4.97 * 10^{-4}$	$1.06 * 10^{-4}$
11.92 : 1.0	0.90	$5.30 * 10^{-4}$	$1.03 * 10^{-4}$
12.98 : 1.0	0.98	$5.62 * 10^{-4}$	$1.00 * 10^{-4}$
14.05 : 1.0	1.06	$5.92 * 10^{-4}$	$9.80 * 10^{-5}$
15.11 : 1.0	1.14	$6.21 * 10^{-4}$	$9.55 * 10^{-5}$
16.17 : 1.0	1.22	$6.47 * 10^{-4}$	$9.32 * 10^{-5}$
17.24 : 1.0	1.30	$6.74 * 10^{-4}$	$9.09 * 10^{-5}$
18.50 : 1.0	1.40	$7.04 * 10^{-4}$	$8.82 * 10^{-5}$
20.00 : 1.0	1.50	$7.32 * 10^{-4}$	$8.57 * 10^{-5}$

2.2.2.3 Electrochemical studies

2.2.2.3.1 General procedure

2.2.2.3.2 Apparatus

All electrochemical experiments were carried out in a three-electrode cell designed in-house comprising of a working electrode, a counter electrode and a reference electrode. The working electrode was a glassy carbon disk with a diameter of 3 mm embedded in Teflon and the counter electrode was a platinum coil. $Ag/AgNO_3$ electrode was used as a reference electrode in DMSO solution.

The counter electrode, platinum wire, was polished with a sandpaper prior to use. A $Ag/AgNO_3$ electrode was customarily constructed by immersing a silver wire into a solution of 0.01 M $AgNO_3$ in 0.1 M supporting electrolyte. The working electrode was polished with slurries of 0.5 μm and 1 μm alumina powder, and washed by sonication for 5 min in 0.05 M sulfuric acid and subsequently with a solvent. Solution was kept under N_2 at all time. Scan rates were at 20, 50, 80, 100, 200, 500, 800 and 1000 mV/s. The appropriated scan rates were found to be 100 mV/s for cyclic voltammetry.

2.2.2.3.3 Chemical

All guest molecules in term of tetrabutylammonium salts and supporting electrolyte, tetrabutylammonium hexafluorophosphate, were dried under reduced pressure overnight. DMSO was dried over CaH_2 overnight and subsequently distilled with CaH_2 under N_2 prior to use.

2.2.2.3.4 Anion studies of L^1H, L^2H and L^3H with NBu_4COOCH_3, $NBu_4COOC_6H_5$, $NBu_4H_2PO_4$, NBu_4Cl, NBu_4F, Ala, Trp and Phe.

Typically, a 1 mM solution of a ligand ($5 * 10^{-3}$ mmol) in 0.1 M supporting electrolyte (5 mL of NBu_4PF_6 in freshly distilled DMSO) was prepared. A stock solution (0.1 M) of an anionic species (0.5 mmol) in supporting electrolyte was prepared. The solution of an anion was added into the solution of the ligand according to the ratios in the Table **2.3**.

Table 2.3 Volumes and moles of NBu_4Cl used for a typical CV experiment

Mole ration Guest : Ligand	Volumn of 0.1 M guest in DMSO	Mole of guest molecule
0.0 : 1.0	0	0
0.2 : 1.0	0.010	$1.00 * 10^{-6}$
0.4 : 1.0	0.020	$2.00 * 10^{-6}$
0.6 : 1.0	0.030	$3.00 * 10^{-6}$
0.8 : 1.0	0.040	$4.00 * 10^{-6}$
1.0 : 1.0	0.050	$5.00 * 10^{-6}$
1.2 : 1.0	0.060	$6.00 * 10^{-6}$
1.5 : 1.0	0.075	$7.50 * 10^{-6}$
1.8 : 1.0	0.090	$9.00 * 10^{-6}$
2.0 : 1.0	0.100	$1.00 * 10^{-5}$
2.5 : 1.0	0.125	$1.25 * 10^{-5}$
3.0 : 1.0	0.150	$1.50 * 10^{-5}$
4.0 : 1.0	0.200	$2.00 * 10^{-5}$

2.3 RESULTS AND DISCUSSION

2.3.1 Synthesis and Characterization of L^1H, L^2H and L^3H

Compounds L^1H and L^2H were synthesized as outlined in scheme 1. A reaction of benzimidazole and *N*-(chloromethyl)phthatimide using K_2CO_3 as base in refluxed acetonitrile gave a white solid which was then reduced by hydrazine in a 2:3 mixture

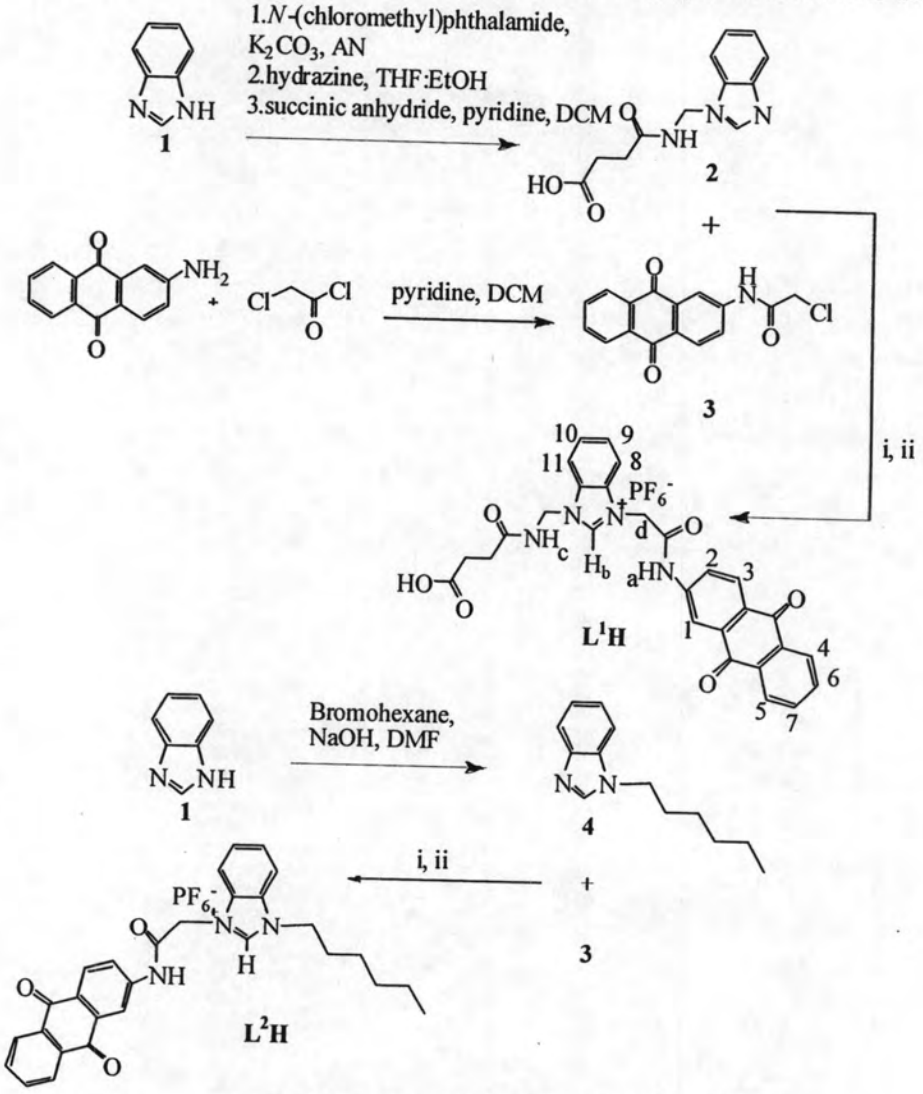

i : NaI, acetone, $CHCl_3$, RT, ii: KPF_6, THF, RT

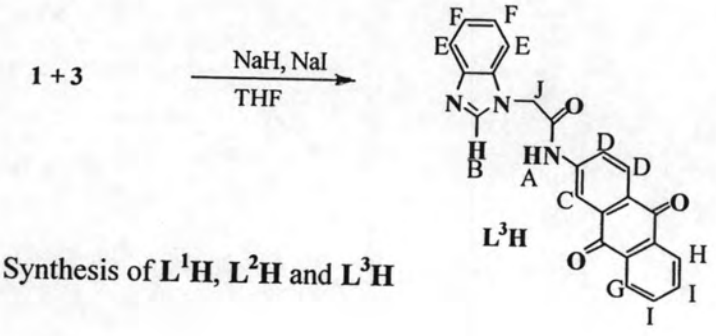

Scheme 2.1. Synthesis of L^1H, L^2H and L^3H

of ethanol:THF and further reacted with succinic anhydride in the presence of pyridine as base in dichloromethane affording 1-*N*-(propanic aminomethyl) benzimidazole (**2**) in 90% yield.

L^1H was obtained in 81% yield by coupling compound **2** with chloroethyleneamido anthraquinone (**3**) followed by anion exchange with KPF_6 in THF. The synthesis of **L^2H** was started by a reaction between benzimidazole and 1-bromohexane using NaOH as base in dimethylformamide at reflux condition to give compound **4** in 80% yield. A coupling reaction of **2** with compound **4** in a mixture of acetone and chloroform in the presence of NaI followed by conversion of counter anions using KPF_6 yielded **L^2H** in 85% yield. **L^3H** was synthesized in 80% yield by coupling benzimidazole with compound **3** using NaH as base in THF.

The structures of **L^1H**, **L^2H** and **L^3H** were characterized by NMR spectroscopy, ESI-MS spectroscopy and elemental analysis. However, the elemental analysis results obtained from experiment were not good agreement with those from calculation since **L^1H** and **L^2H** are in form of salts, which are very hygroscopic when exposed in air. From ^{1}H-NMR spectra, the characteristic peaks namely, the N*H*$_{amide}$ on anthraquinone , C(2)*H*, and -N$_{imid}$C*H*$_2$N$_{amide}$- of **L^1H** and **L^2H** displayed at 11.22 and 11.30 ppm, 8.466 and 9.78 ppm as well as 5.47 and 5.60 ppm, respectively. In the case of **L^3H**, the N*H*$_{amide}$ on anthraquinone group and C(2)*H* shows at 11.131 and 8.449 ppm, respectively. Moreover, only **L^1H** contains the carboxylic group on side chain, therefore, it has the N*H*$_{car}$ proton positioned at 9.26 ppm as shown in Figure 2.1.

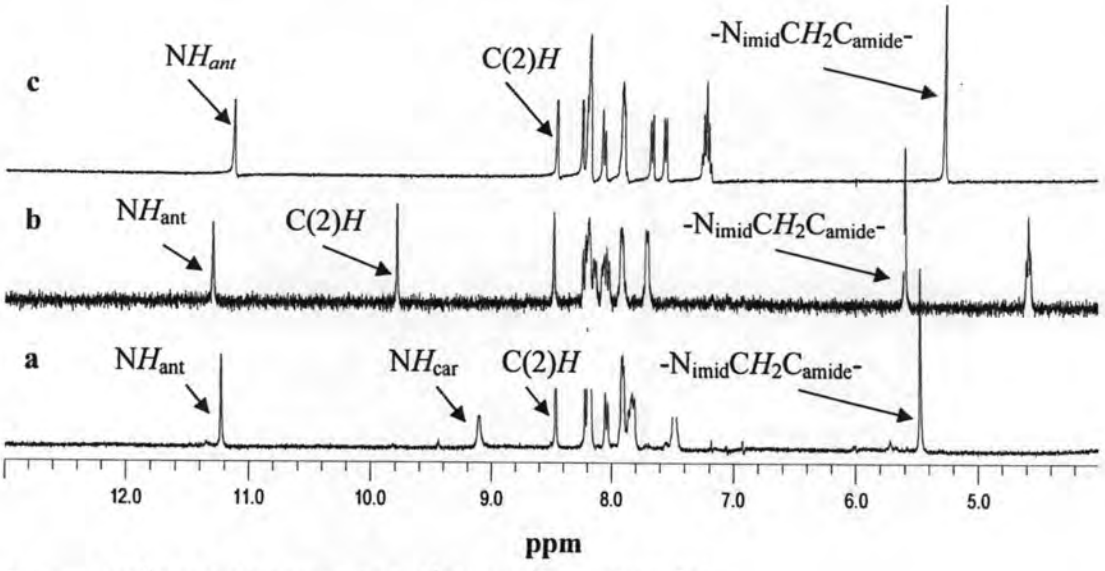

Figure 2.1 ^{1}H NMR specta of a) **L^1H**, b) **L^2H** and c) **L^3H**.

2.3.2 Binding properties of L^1H, L^2H and L^3H

2.3.2.1 The complexation studies of the synthesized compounds with various anion and amino acids by ^1H NMR spectroscopy

Binding studies of $\mathbf{L^1H}$ and $\mathbf{L^2H}$ towards F^-, Cl^-, Br^-, $H_2PO_4^-$, AcO^-, BzO^-, Trp, Phe and Ala were carried out by NMR spectroscopy in DMSO-d_6. Figure 2.2 showed ^1H-NMR spectra relied on the complexation of $\mathbf{L^1H}$ and all guests at 5 equivalents. Upon addition of 5 equiv. Cl^- and Br^- of $\mathbf{L^1H}$, it was found that protons of NH_{ant} and NH_{car} at peak a and c were downfield shift and C(2)H at peak b showed a small downfield shift due to hydrogen bonding and the aromatic region displayed the significant changes. Concerning the addition of F^-, AcO^-, BzO^- and $H_2PO_4^-$ to $\mathbf{L^1H}$, the NH_{ant} and NH_{car} resonances disappeared in the spectra. The first assumption is that both NH-amide proton are attributed to the deprotonation process.[49-54] Otherwise, it is probably due to the occurrence of the strong hydrogen bonding interaction with anions (carboxylate, F^- and $H_2PO_4^-$) resulting in the weak covalent interaction between N and H atoms of amide groups. Interestingly, NH_{car} resonance in the case of $\mathbf{L^1H}$ with 5 equiv. Trp was not observed but NH_{ant} resonace still appeared at downfield shift even though the latter proton is more acidity than the former proton. It was revealed that NH_{ant} proton did not rely on only the deprotonation process. It was induced the occurrence of the hydrogen bonding interaction between carboxylate of Trp and NH_{ant}. In all cases of guests, the C(2)H protons retained the appearance at the low field resonance in the attribution of hydrogen bonding interactions. Except for F^-, this peak is the existence of a high field at 8.225 ppm ($\Delta\delta$ = -0.241 ppm). Moreover, all peaks of aromatic and CH_2 protons dramatically shifted to upfield possibly caused by the enhancement of the negative charge to aromatic system from the deprotonated amide proton adjacent to anthraquinone. Their peaks would be splitted and not similar to the initial $\mathbf{L^1H}$ because – NH_{car} –CH_2-N_{imi}- might be cleaved by strong bases such as F^-, AcO^-, BzO^- and $H_2PO_4^-$.[49-51] The structure of $\mathbf{L^1H}$ would be changed to $\mathbf{L^3H}$ by observing the spectrum pattern whose the aromatic region performed at the same chemical shift as the unbound $\mathbf{L^3H}$. From ^1H-NMR spectrum of $\mathbf{L^1H}$ with F^-, $H_2PO_4^-$, AcO^- and BzO^- showed that these anions can cleave at – NH_{car}CH_2N$_{imi}$- and deprotonate at NH_{ant}.

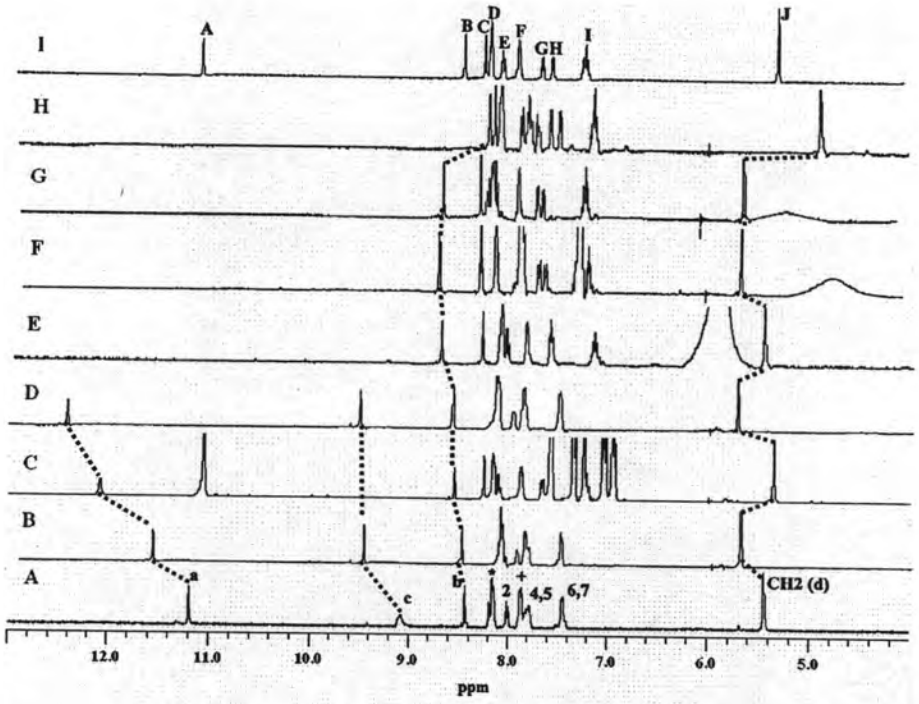

* assignments of protons at 1,3, 8 and 11 ; $^{+}$ assignments of protons at 9 and 10

Figure 2.2. ^{1}H-NMR spectrum in DMSO-d_6 at 298 K of A) **L^{1}H** (5 * 10^{-3} M), B) **L^{1}H** + 5 equiv.Bu_4NBr, C) **L^{1}H** + 5 equiv. Trp, D) **L^{1}H** + 5 equiv. Bu_4NCl and E) **L^{1}H** + 5 equiv. $Bu_4NH_2PO_4$ F) **L^{1}H** + 5 equiv. Bu_4NBzO G) **L^{1}H** + 5 equiv. Bu_4NAcO
H) **L^{1}H** + 5 equiv. Bu_4NF and I) **L^{3}H**

To support the hypothesis about the cleavage of – N*H*$_{car}$ –C*H*$_2$-N$_{imi}$- for **L^{1}H,** it was confirmed by Mass Spectroscopy shown as Figure 2.3. The mass result of **L^{1}H** in the presence of 5 equiv. Bu_4NF showed m/z at 381.678 corresponding to the cleaved structure at –N*H*$_{car}$ –CH$_2$-N$_{imi}$- of **L^{1}H** and is agreement with MS of **L^{3}H.** Additionaly, to prove this hypothesis about the cleavage process, **L^{3}H** was synthesized to be the control compound and then was studied on complexed behavior toward various anions and amino acids illustrated in Figure 2.4. Upon addition of 5 equiv. of anions into **L^{3}H** solution, it was found that N*H* at A position of anthraquinone diappeared caused by deprotonation. But –C(2)*H* – of **L^{3}H** was slightly shifted to downfield similarly to **L^{1}H** with these anions due to hydrogen bonding interaction.

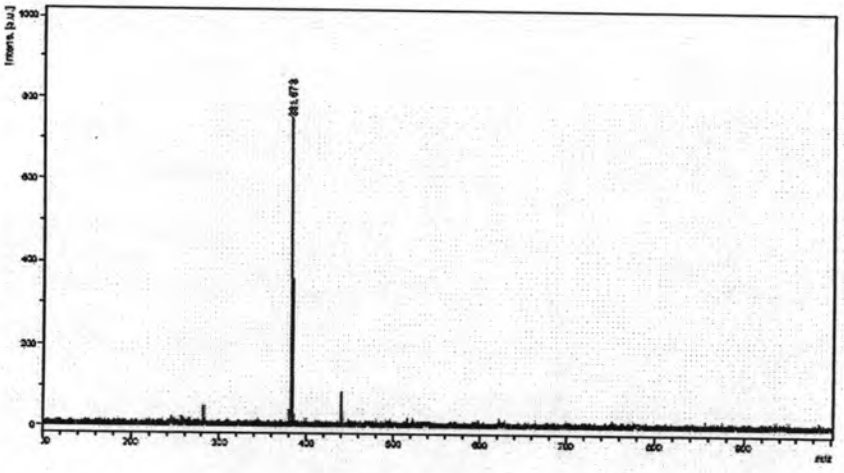

Figure 2.3. Mass spectrum of $\mathbf{L^1H}$ with 5 equiv. Bu_4NF in DMSO

We took attempt to find the association constant of $\mathbf{L^3H}$ toward anions and amino acids. Unfortunately, they couldnot be obtained because of unsuiTable shape for hydrogen bonding interaction between C(2)*H* anions. Moreover, proton on NH_{ant} was deprotonated by anions resulting in the suppression of the hydrogen bonding interaction with anions.

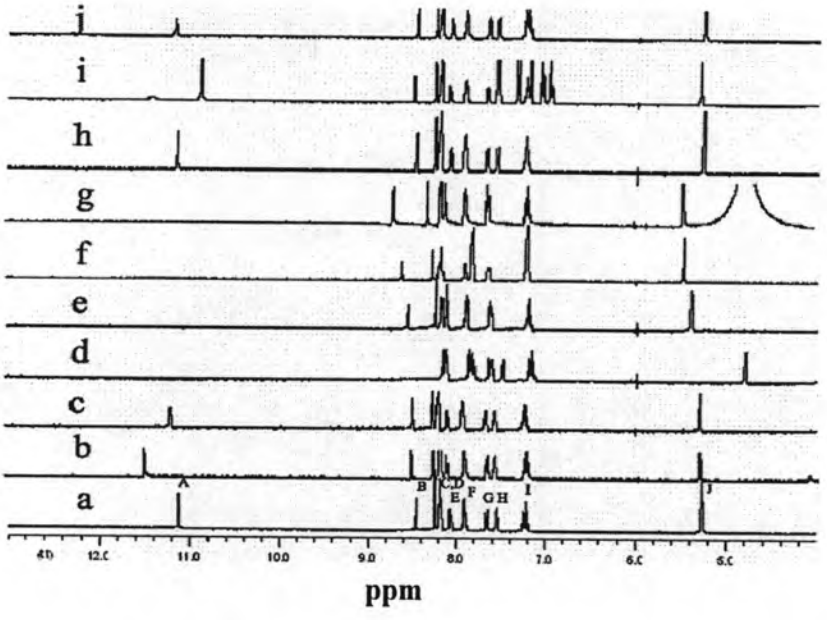

Figure 2.4. ^{1}H-NMR spectrum in DMSO-d_6 at 298 K of a) $\mathbf{L^3H}$ ($5 * 10^{-3}$ M), b) $\mathbf{L^3H}$ + 5 equiv.Bu_4NCl, c) $\mathbf{L^3H}$ + 5 equiv. Bu_4NBr, d) $\mathbf{L^3H}$ + 5 equiv. Bu_4NF and e) $\mathbf{L^3H}$ + 5 equiv. Bu_4NAcO f) $\mathbf{L^3H}$ + 5 equiv. Bu_4NBzO g) $\mathbf{L^3H}$ + 5 equiv. $Bu_4N\ H_2PO_4$ h) $\mathbf{L^3H}$ + 5 equiv. Ala i) $\mathbf{L^3H}$ + 5 equiv. Trp and j) $\mathbf{L^3H}$ + 5 equiv. Phe.

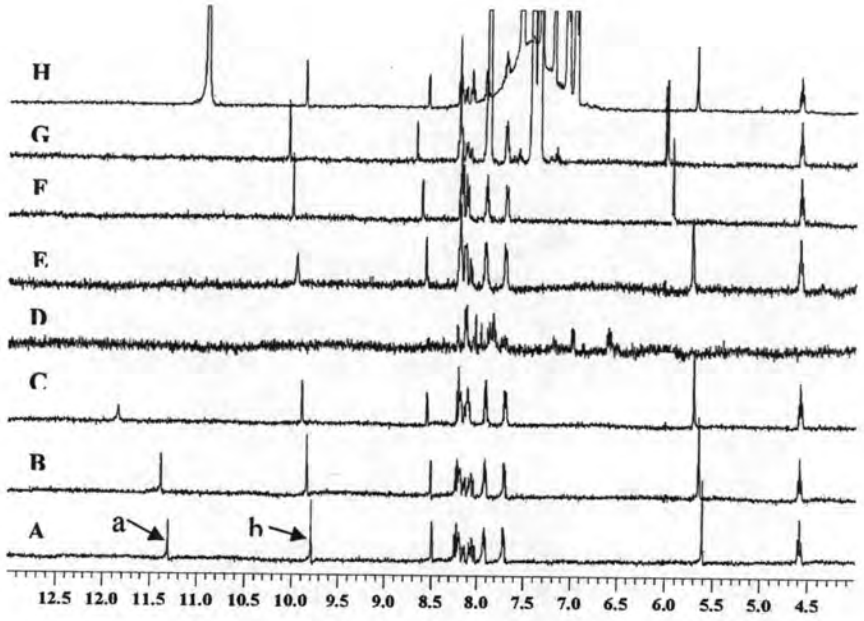

Figure 2.5. ^{1}H-NMR spectrum in DMSO-d_6 at 298 K of A) $\mathbf{L^2H}$ ($5 * 10^{-3}$ M), B) $\mathbf{L^2H}$ + 5 equiv.Bu_4NBr, C) $\mathbf{L^2H}$ + 5 equiv. Bu_4NCl, D) $\mathbf{L^2H}$ + 5 equiv. Bu_4NF and E) $\mathbf{L^2H}$ + 5 equiv. Bu_4NAcO F) $\mathbf{L^2H}$ + 5 equiv. $Bu_4N\ H_2PO_4$ G) $\mathbf{L^2H}$ + 5 equiv. Bu_4NBzO and H) $\mathbf{L^2H}$ + 5 equiv. Trp.

Figure 2.5 showed the ^{1}H-NMR spectrum of $\mathbf{L^2H}$ with 5 equiv. various anions and amino acids. In the case of Br^- and Cl^-, N*H* and C(2)*H* peaks at a and b position were shifted to downfield due to hydrogen bonding and the aromatic region was slightly changed. In the presence of AcO^-, BzO^- and $H_2PO_4^-$, the N*H* was disappeared because these anions are able to deprotonate N*H* at anthraquinone of $\mathbf{L^2H}$. It was found that these anions can not clevaged bond at $-CH_2N_{imi}-$ of $\mathbf{L^2H}$ but only deprotonated NH of anthraquinone because the $-CH_2N_{imi}-$ was still displayed at about 4.57 ppm in the spectrum 2.5E-G. Upon addition F^-, the spectrum was shifted to upfield because of the enhancement negative charge in the system. Moreover, F^- can deprotonate the N*H* at anthraquinone of $\mathbf{L^2H}$. Additional, the carboxylated group Trp has ability to deprotonate N*H* at the anthraquinone shown in Figure 2.5H.

Moreover, we can conclude that $\mathbf{L^2H}$ and base: F^-, AcO^-,BzO^- and $H_2PO_4^-$ underwent the depronation proton but not the cleavage process. From ^{1}H NMR titration of $\mathbf{L^1H}$ and $\mathbf{L^2H}$ with various anions and amino acids, it was found that the NH_{ant} signal

of $\mathbf{L^1H}$ was disappeared upon addition 0.8, 1.0, 1.6 and 2.0 equiv. of F^-, AcO^-, BzO^- and $H_2PO_4^-$, respectively. While this signal of $\mathbf{L^2H}$ was vanished 0.1, 0.1, 0.1 and 2.5 equiv.of F^-, AcO^-, BzO^- and $H_2PO_4^-$, respectively.

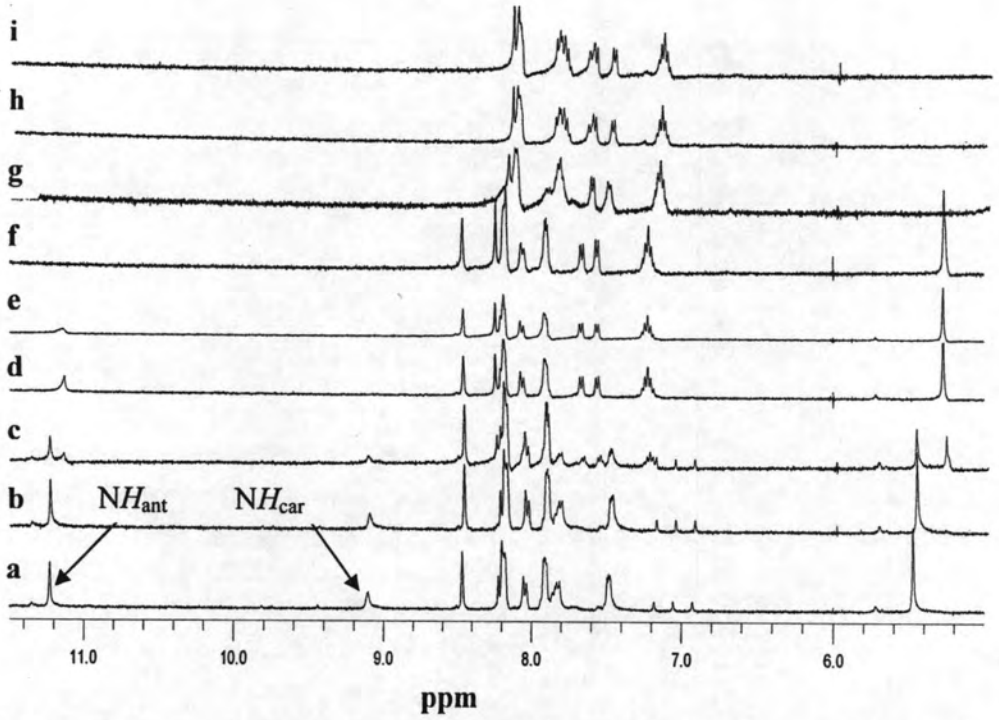

Figure 2.6. The disappeared NH_{ant} and NH_{car} of L^1H (5 * 10^{-3} M) with various ratios of Bu_4NF a) 1:0, b) 1:0.1, C) 1:0.2, d) 1:0.3, e) 1:0.4, f) 1:0.5, g) 1:1, h) 1:2, i) 1:3

In the case of the NH_{car} resonance belonging to $\mathbf{L^1H}$ vanished at 0.4 equiv. F^-, 0.4 equiv. AcO^-, 0.6 equiv. BzO^- and 0.4 equiv. $H_2PO_4^-$ and shown in Figure 2.6. Amount of anions added into $\mathbf{L^1H}$ and $\mathbf{L^2H}$ induced the disappear of some signal listed in the Table 2.1.

Table 2.4. The equivalents of guests effect on the disappear of signal of $\mathbf{L^1H}$ and $\mathbf{L^2H}$ using ^{1}H-NMR spectroscopy

Anions	$\mathbf{L^1H}$		$\mathbf{L^2H}$
	NH_{ant}	NH_{car}	NH
F^-	0.8	0.4	0.1
CH_3COO^-	1.0	0.4	0.1
$C_6H_5COO^-$	1.6	0.6	0.1
$H_2PO_4^-$	2.0	0.4	2.5

The features of spectra for the bound ligand differ from the pattern of spectrum for the unbound ligand indicating that $\mathbf{L^1H}$ can bind with all guests with the different binding abilities in the dependent on size and geometry of anions, mainly on the basicity.

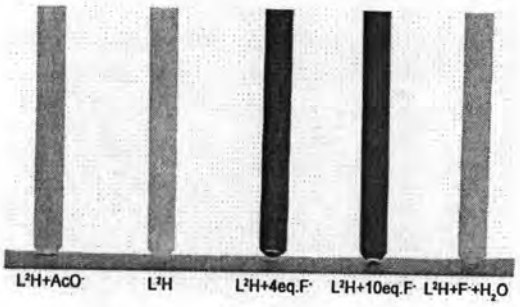

Figure 2.7. The colour change of $\mathbf{L^2H}$ were observed under each condition in DMSO.

Concomitant with deprotonation, dramatic color changes were observed upon addition of F^- and AcO^- to $\mathbf{L^1H}$ and $\mathbf{L^2H}$. In the presence of 4 equiv. AcO^-, the color of the solution was changed from yellow to orange and further addition of F^- shifted the colour to deep red (Figure 2.7). However, the color change is less intense in the case of AcO^-. This is probably due to the stronger base character of F^-. Upon addition of H_2O, the red color of $\mathbf{L^2H{\bullet}F^-}$ turned to the initial color (Figure 2.7). This signified that the deprotonation of $\mathbf{L^2H}$ is reversible in a similar fashion to $\mathbf{L^1H}$. Considering the case of BzO^-, $H_2PO_4^-$, the color changes slightly, thus we could not observe significantly. Unlike the cases of Br^-, Cl^-, Trp, Phe and Ala, the color changes could not be observed with naked-eyes. According to ^{1}H-NMR data for ligand and these guests, the NH_{ant} still appeared in spectra and subsequently the charge transfer of electron from N atom to anthraquinone did not take place obviously. We couldn't calculate the binding constant

from ^{1}H NMR titration because the **L^{1}H** probably underwent deprotonation and cleavage precess but the **L^{2}H** was deprotonated with strong base such as F^-, AcO^-,BzO^- and $H_2PO_4^-$. Therefore, we calculated the binding constant from UV-vis technique.

2.3.2.2 The complexation studies of synthesis compounds with various anion and amino acids by UV-visible spectroscopy

From ^{1}H NMR studies of **L^{2}H** with Bu_4NCH_3COO and Bu_4NF, the colour was changed from yellow to orange and red, respectively. Interestingly, the colour changes related to the red-shift of absorption band.Moreover, upon addition of H_2O in the **L^{2}H** + F^-, the colour was turned to be yellow colour as shown in Figure 2.7.

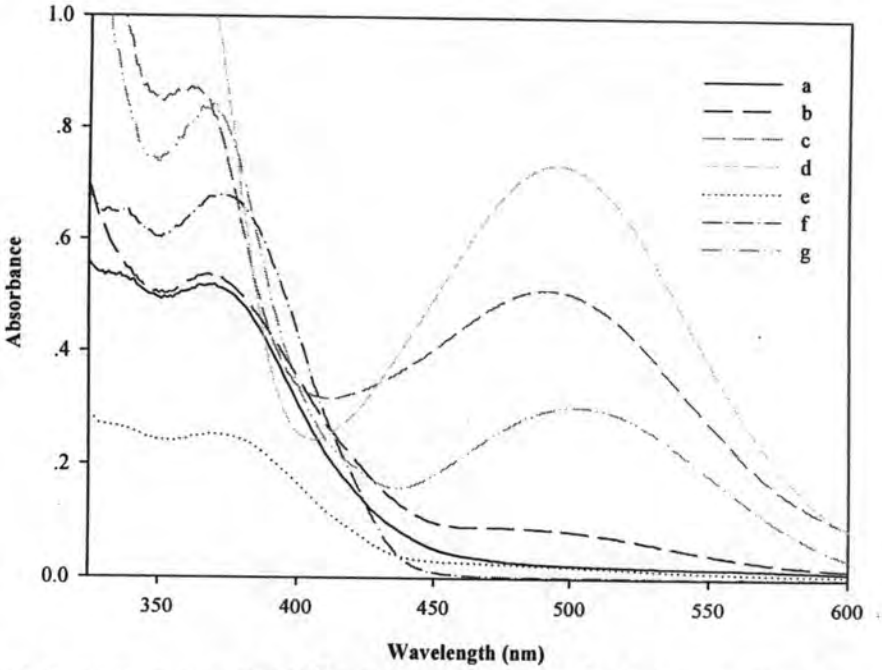

Figure 2.8. UV spectra of a) **L^{1}H** ($1.5 * 10^{-4}$M), b) **L^{1}H** + 4 equiv. Bu_4NF, c) **L^{2}H** ($7.5 * 10^{-4}$M), d) **L^{2}H** + 4 equiv. Bu_4NF, e) **L^{2}H** + Bu_4NCH_3COO f) **L^{2}H** + 4 equiv. Bu_4NOH, g) **L^{2}H** + 4 equiv. Bu_4NF + ex. H_2O in DMSO at 298 K.

The deprotonation process was found to be completely reversible, since **L^{2}H**•F^- showed the original color and spectrum of **L^{2}H** in the presence of H_2O (blue line in Fig. 2.8g).

Additionally, upon addition of Bu_4NOH in **L^{2}H**, the colour of solution was changed from yellow to red. The colour change of Bu_4NOH is similar to in the case of F^-.

This result is agreed with Fabbrizzi's result about the deprotonation process using strong base.[56]

The UV-vis spectra of ligand $\mathbf{L^1H}$ in DMSO [$1.5 * 10^{-4}$] was observed and shown in Figure 2.9. Free ligand $\mathbf{L^1H}$ showed a maximum absorption band at 373 nm. Considering the titration of $\mathbf{L^1H}$ with various anions and amino acids, upon addition of Cl^-, Br^-, $C_6H_5COO^-$, $H_2PO_4^-$, Ala, Trp and Phe, the absorption band at 373 nm was slightly decreased. But in the case of AcO^- and F^-, this band would be decreased and found a new at 489 nm because the negative charge enhance π delocalization on anthraquinone and stabilized the energy of the π- π* transition.[44-46, 55] When a new band was found at 489 nm, the colour was changed from yellow to red. But in the presence of AcO^-, the colour would be changed from yellow to orange because the AcO^- is less base than F^-.(illustrated in Figure 2.8.)

a)

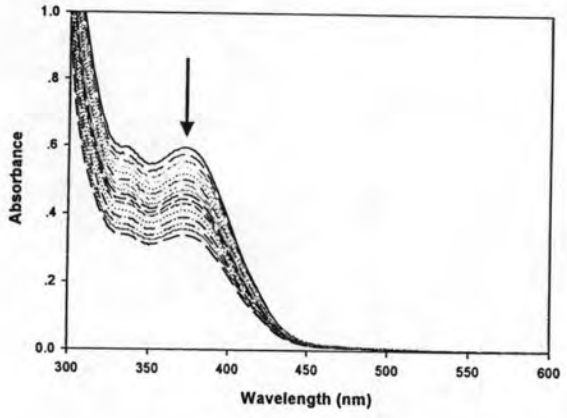

b)

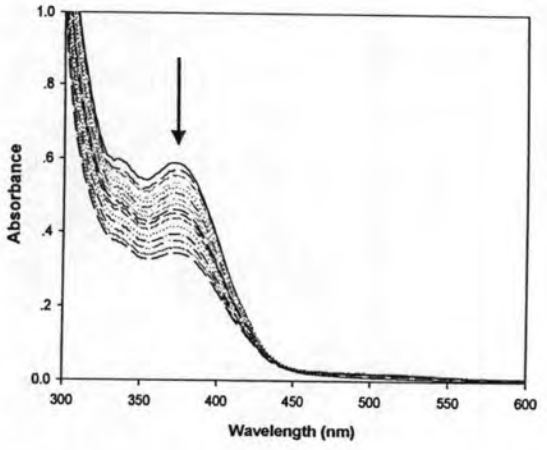

Figure 2.9. UV titration of $\mathbf{L^1H}$ = $1.5 * 10^{-4}$ M with a) Bu_4NCl = 0-0.004 M in DMSO. b) Bu_4NCH_3COO = 0-0.004 M

From UV titration of $\mathbf{L^1H}$ with various anions and amino acids, we can not calculate the association constant because $\mathbf{L^1H}$ was clevaged at the $-N_{amide}CH_2N_{imi}-$ and deprotonated N*H* at anthraquinone.

The UV-vis spectra of ligand $\mathbf{L^2H}$ in DMSO [$7.5 * 10^{-4}$] was observed and shown in Figure 2.10.

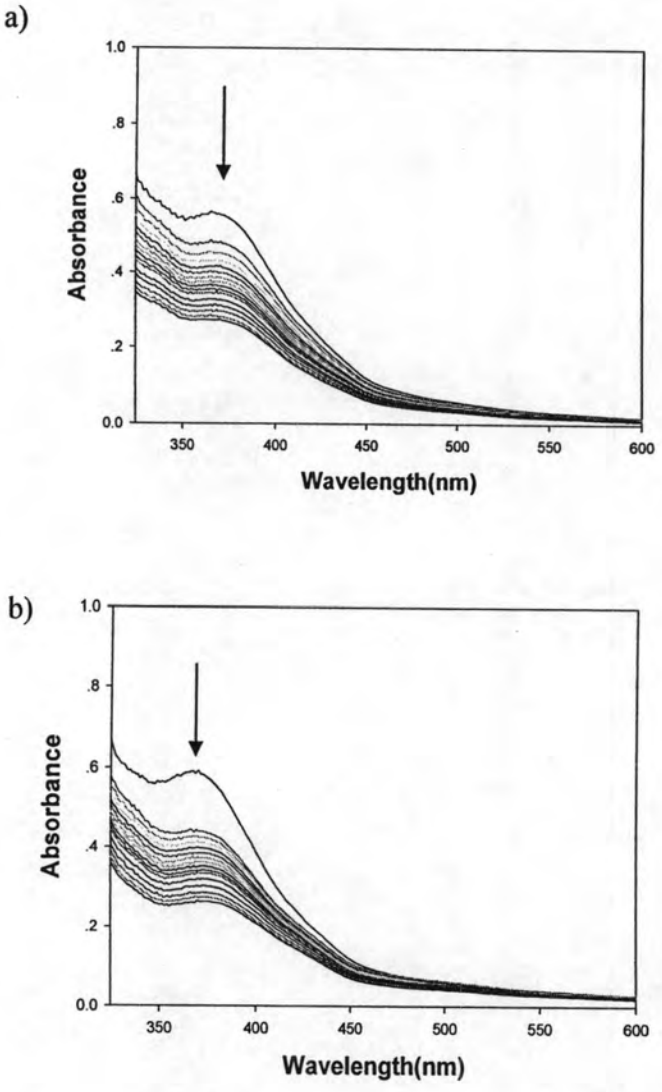

Figure 2.10. UV titration of $\mathbf{L^2H}$ = $7.5 * 10^{-4}$ M with a) Bu_4NCl = 0-0.004 M in DMSO. b) $Bu_4NC_6H_5COO$ = 0-0.004 mL

Free ligand displayed a absorption band at 370 nm. It was found that upon addition of Cl^-, Br^-, $C_6H_5COO^-$ and $H_2PO_4^-$, Ala, Trp and Phe, the absorption band at 370 nm was decreased. In the presence of AcO^- and F^-, this band would decrease with a

concomitant of the appearance of a new at 489 nm due to the enhancement of π-delocalization on anthraquinone resulting in stabilization of the energy of the π- π* transition.[41-46, 55]

a)

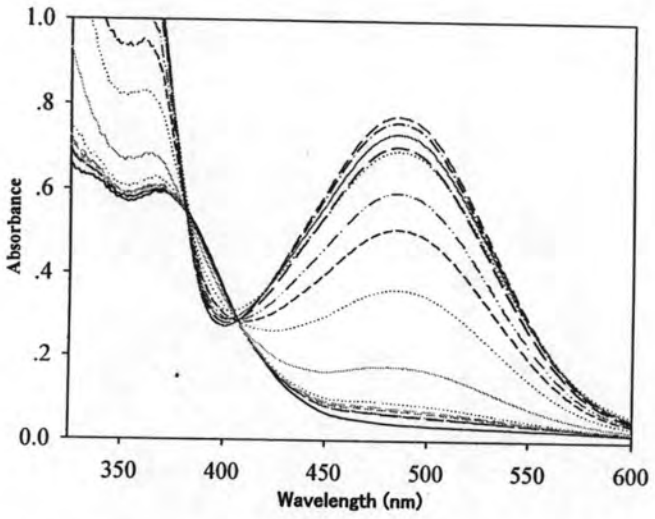

b)

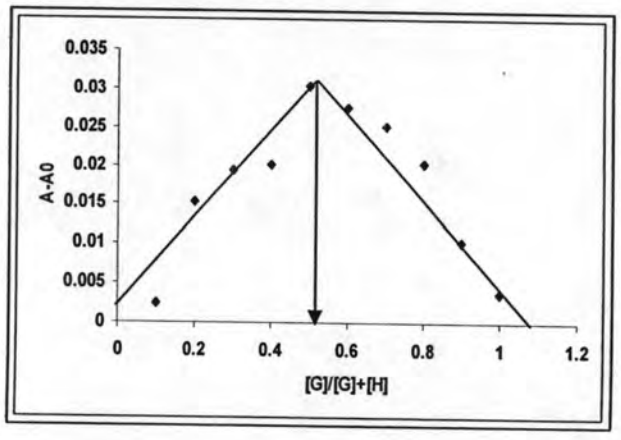

Figure 2.11. UV titration of $\mathbf{L^2H}$ = 7.5 * 10^{-4} M with a) Bu_4NF = 0-0.004 M (b) Job's plot of $\mathbf{L^2H}$ and Bu_4NF.

Binding constants of receptors $\mathbf{L^2H}$ towards anions were measured by UV-visible titrations in DMSO. The titration curve of $\mathbf{L^2H}$ with F^- was shown in Figure 3.8(a). Job's plot measured by UV technique indicated that ligands bind anions in a 1:1 fashion. The results are analogue with the case of $\mathbf{L^2H}$ towards other guests. All log K values were calculated by Spectfit 32 program in the model of 1:1 complexation and collected in Table 2.2.

Table 2.5. Binding constants for 1:1 complexes of $\mathbf{L^2H}$ with various anions and amino acids in DMSO at 298 K

Anion	F^-	Cl^-	Br^-	$H_2PO_4^-$	CH_3COO^-	$C_6H_5COO^-$	Ala	Trp	Phe
log K[a]	-[c]	3.71[b]	3.63[b]	4.22	-[c]	5.63	-[c]	-[c]	-[c]

[a]log *K* values have an error < 10%. [b]The log K_1 value refers to H-bonding with Cl^-, and Br^- calculated at 300-400 nm. [c]log *K* values cannot be calculated.

The selectivity of $\mathbf{L^2H}$ is in trend $Br^-<Cl^-<H_2PO_4^-<C_6H_5COO^-$. The results show that $\mathbf{L^2H}$ appreciated Y-shape anions better than spherical anions. The association constant of $\mathbf{L^2H}$ towards benzoate is higher than acetate probably due to π-π stacking interactions. However, the association constants of $\mathbf{L^2H}$ toward $F^-$and AcO^- could not be refined. F^- and AcO^- can abstract the NH_{ant} proton of $\mathbf{L^2H}$ immediately and thus, the binding process would not occur. Moreover, log K values of ligand toward amino acids could not be obtained because the structure of $\mathbf{L^2H}$ does not contain the unit which is a able to bind $-NH_3^+$ group of zwitterionic amino acid and has unsuiTable shape for amino acid.

Complexation studies of $\mathbf{L^3H}$ towards anions and amino acids, it was found that the absorption band of $\mathbf{L^3H}$ is similar to $\mathbf{L^2H}$ but we could not calculate the binding constant because the binding site of $\mathbf{L^3H}$ was not suiTable and selective with shape of anions and amino acids so it is difficult to preorganize the structure prior to bind with guest.

2.3.2.3 The complexation studies of synthesis compounds with various anions and amino acids by cyclic voltammetry

$\mathbf{L^1H}$, $\mathbf{L^2H}$ and $\mathbf{L^3H}$ have a unit of anthraquinone in their molecule. Normally, the anthraquinone exhibits two redox couples whose reversible first wave represents an electron transfer of the quinone moiety (AQ) to form a semiquinone anion radical (AQ^-). The second irreversible reduction wave corresponds to the subsequent addition of a second electron to the semiquinone anion radical, producing a hydroquinone dianion

(AQ^{2-}). This is reasonable to study the electrochemical properties of the $\mathbf{L^1H}$, $\mathbf{L^2H}$ and $\mathbf{L^3H}$ with anions and amino acids.

Therefore, the electrochemical properties of this ligand can be studied using cyclic voltammetry and square wave. The cyclic voltammetry was performed using solution of $\mathbf{L^1H}$, $\mathbf{L^2H}$ and $\mathbf{L^3H}$ in distilled anhydride dimethysulfoxide with 0.1 M Bu_4NPF_6 as supporting electrolyte and using a glassy carbon as working as electrode, a Ag^+ as reference electrode and a Pt wire as counter electrode. All solution was purged with N_2 before measurement. The potential was scanned in the range from 0 to -2.0 V at 100 mV/s. The cyclic voltammograms of $\mathbf{L^1H}$, $\mathbf{L^2H}$ and $\mathbf{L^3H}$ was shown in the Figure 2.12. The values of the potential were listed in Table 2.3.

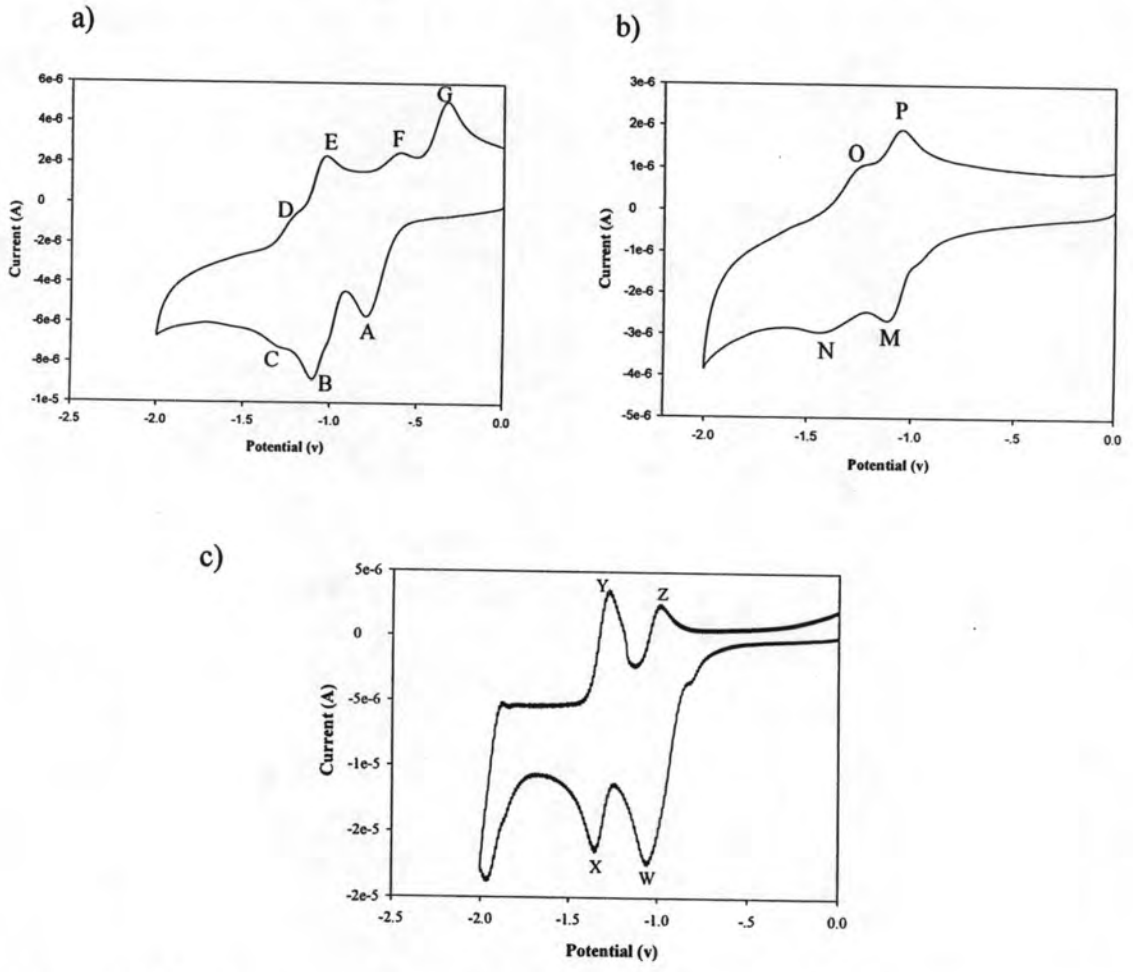

Figure 2.12 Cycic voltammogram of a) $\mathbf{L^1H}$, b) $\mathbf{L^2H}$ and c) $\mathbf{L^3H}$ in dimethylsulfoxide with 0.1 M Bu_4NPF_6

Table 2.6 The characteristic values of L^1H, L^2H and L^3H

Ligands	E_{pc} (V) A, M, W	E_{pc} (V) B, N, X	E_{pc} (V) C	E_{pa} (V) D, O, Y	E_{pa} (V) E, P, Z	E_{pa} (V) F	E_{pa} (V) G
L^1H	-0.854	-1.099	-1.364	-1.239	-1.047	-0.546	-0.244
L^2H	-1.083	-1.392	-	-1.257	-1.041	-	-
L^3H	-1.011	-1.345	-	-1.270	-0.991	-	-

All Cyclic voltammograms measurements of the free L^1H, L^2H and L^3H were carried out by varied scan rates at 20, 50, 80, 100, 200, 500, 800 and 1000 mV/s. Cyclic voltammograms of L^1H, L^2H and L^3H at various scan rates in dimethylsulfoxide are shown in Figure 2.13. The correlation between current (i) and square root of scan rates ($\nu^{1/2}$) was plotted and shown in Figure 2.14. The plot of i_p and $\nu^{1/2}$ is a straight line. It is inductive of disffusion mechanism for L^1H .(Figure 2.13a) In the case of L^2H and L^3H, the plot of i_p and $\nu^{1/2}$ of the first reduction of compound L^2H and L^3H are non-linear indicating that the electron transfer of L^2H and L^3H undergoes the adsorption process. (shown in Fig 2.14)

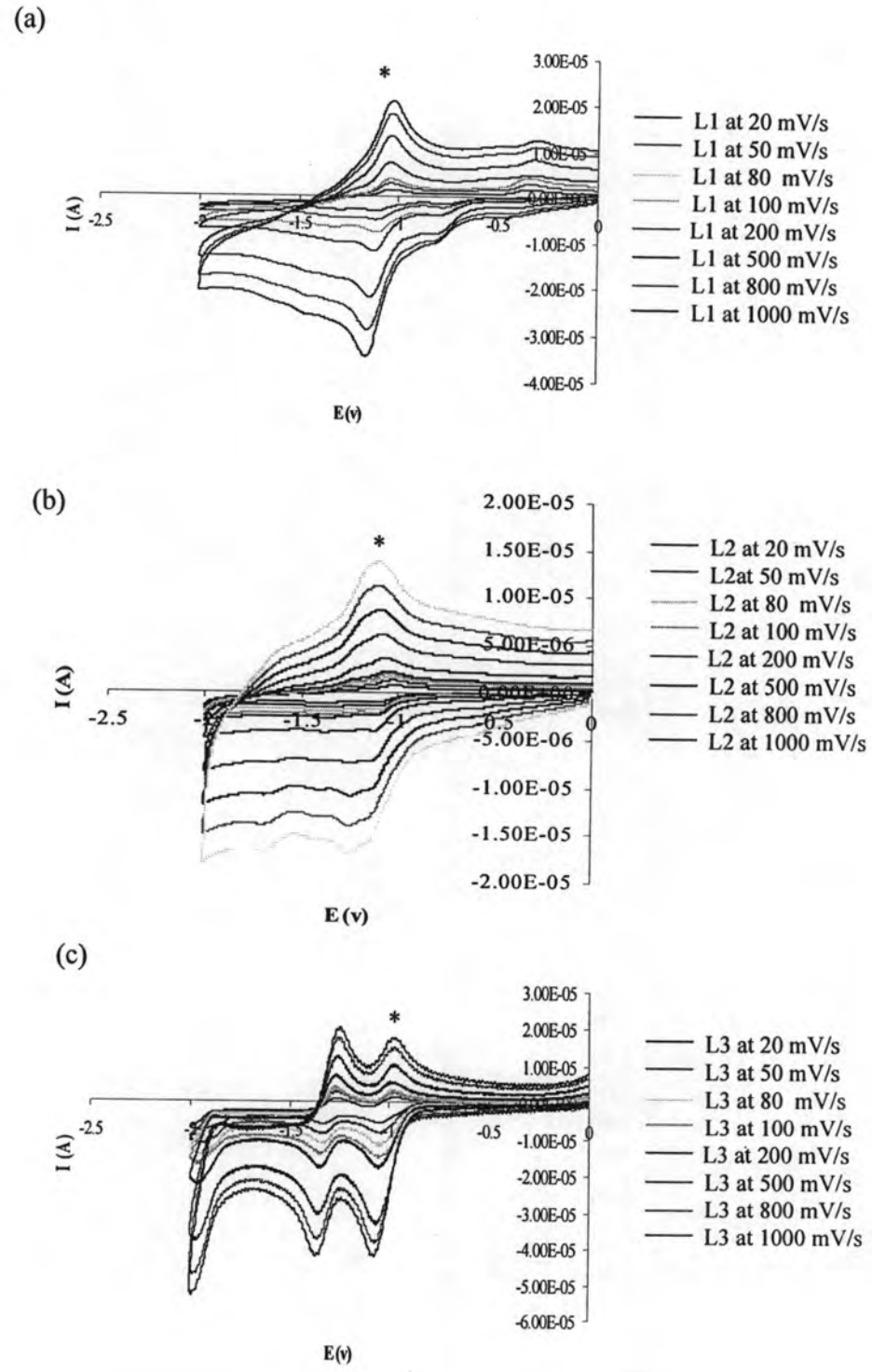

*- This peak was used to plot of i_p and $\nu^{1/2}$

Figure 2.13 Cyclic voltammograms of $\mathbf{L^1H}$ (a), $\mathbf{L^2H}$ (b) and $\mathbf{L^3H}$ (c) in DMSO with 0.1 M TBAPF at different scan rates

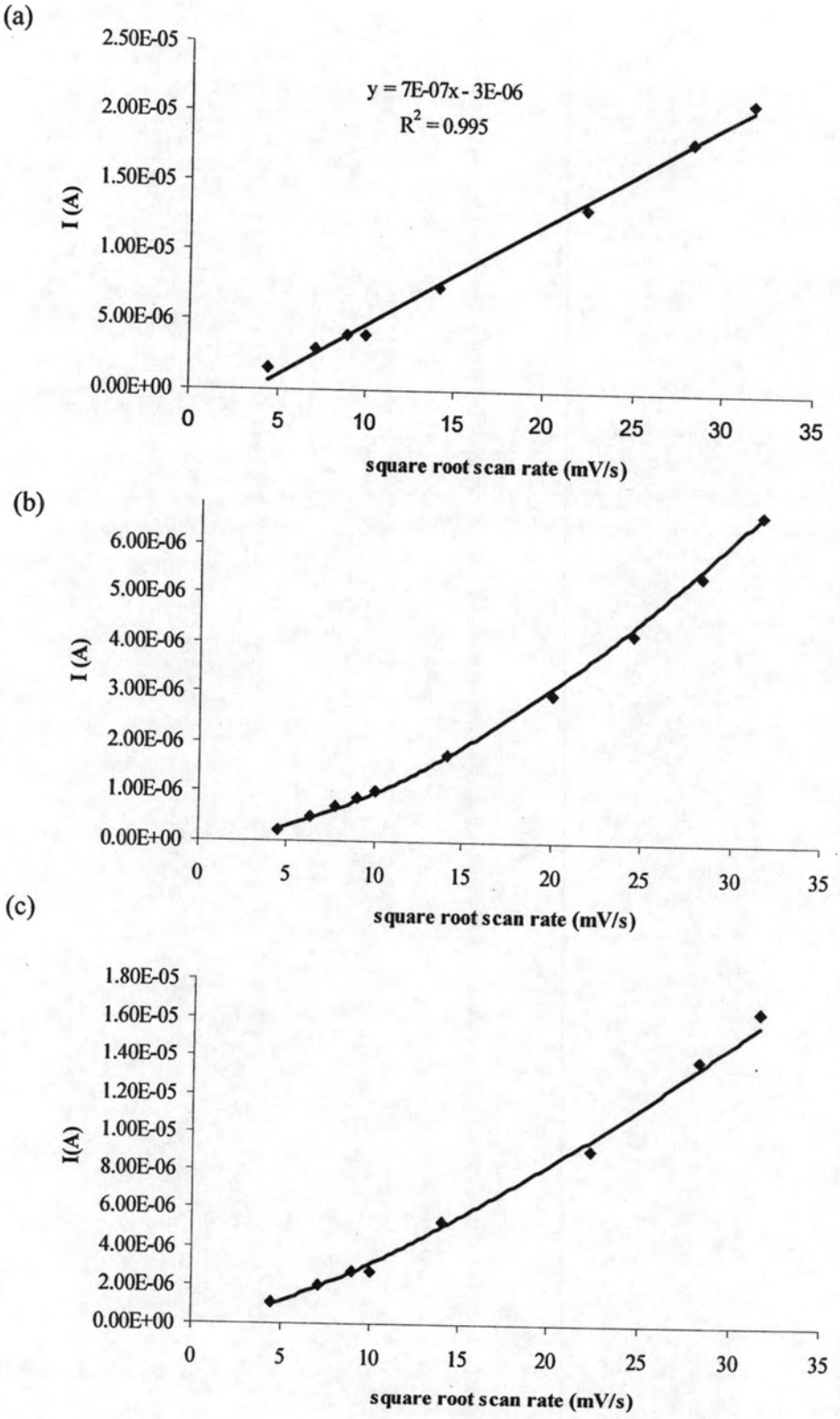

Figure 2.14 Plots of current (i) and square root of scan rates ($\nu^{1/2}$) for $\mathbf{L^1H}$ (a), $\mathbf{L^2H}$ (b) and $\mathbf{L^3H}$ (c) in DMSO

Table 2.7 The potential values of compound L^2H with various guests

	E_{pc}(V) M, M1-8	E_{pc}(V) N, N1-8	E_{pa}(V) O, O1-8	E_{pa2}(V) P, P1-8	ΔE_{pc}(V) M-M1-8	ΔE_{pc}(V) N-N1-8	ΔE_{pa}(V) O-O1-8	ΔE_{pa}(V) P-P1-8
L^2H	-1.083	-1.392	-1.257	-1.041	-	-	-	-
+ Cl^-	-1.083	-	-1.038	-1.251	0	-	-0.219	0.200
+ F^-	-1.193	-1.443	-1.352	-1.120	0.110	0.051	0.095	0.079
+ $H_2PO_4^-$	-1.099	-	-0.967	-	0.0160	-	-0.290	-
+ CH_3COO^-	-1.077	-	-	-0.983	-0.006	-	-0.274	-0.058
+$C_6H_5COO^-$	-0.970	-1.047	-0.784	-	-0.113	-0.345	-0.473	-
+ Ala	-1.083	-	-1.013	-0.519	0	-	-0.244	-0.522
+ Trp	-1.080	-	-0.882	-	-0.003	-	-0.375	-
+ Phe	-1.031	-	-0.977	-0.479	-0.052	-	-0.280	-0.562

(1 = Cl^-, 2 = F^-, 3 = $H_2PO_4^-$, 4 = CH_3COO^-, 5 = $C_6H_5COO^-$, 6 = L-Ala, 7 = L-Trp and 8 = L-Phe)

Table 2.8 The potential values of compound L^3H with various guests

	E_{pc}(V) W	E_{pc}(V) X	E_{pc}(V) S	E_{pa}(V) Y	E_{pa}(V) Z	E_{pa}(V) T	ΔE_{pc}(V) W-W1-8	ΔE_{pc}(V) X-X1-8	ΔE_{pc}(V) S-S3	ΔE_{pa}(V) Y-Y1-8	ΔE_{pa}(V) Z-Z1-8	ΔE_{pa}(V) T-T3
L^3H	-1.011	-1.345	-	-1.270	-0.991	-	-	-	-	-	-	-
+ Cl^-	-1.011	-1.333	-	-1.257	-0.981	-	0	-0.012	-	-0.013	-0.01	-
+ F^-	-1.057	-1.333	-	-1.262	-0.977	-	0.046	-0.012	-	-0.008	-0.014	-
+ $H_2PO_4^-$	-1.028	-1.304	-1.624	-1.470	-1.204	-1.018	0.017	-0.041	1.624	0.200	0.213	1.018
+ CH_3COO^-	-1.006	-1.335	-	-1.260	-0.972	-	-0.005	-0.01	-	-0.257	-0.019	-
+ $C_6H_5COO^-$	-1.011	-1.321	-	-1.257	-0.969	-	0	-0.024	-	-0.388	-0.022	-
+ L-Ala	-1.030	-1.362	-	-1.265	-0.989	-	0.019	0.0017	-	-0.005	-0.002	-
+ L-Trp	-1.050	-1.382	-	-1.279	-0.991	-	-0.039	0.0037	-	0.009	0	-
+D-Trp	-0.979	-1.133	-	-1.028	-	-	-0.032	-0.212	-	-0.242	-	-
+ L-Phe	-1.006	-1.162	-	-	-0.986	-	-0.005	-0.183	-	-1.270	-0.005	-
+ D-Phe	-0.938	-1.106	-1.360	-	-0.994	-	-0.073	-0.2.39	1.360	-1.270	-0.003	-

(1 = Cl^-, 2 = F^-, 3 = $H_2PO_4^-$, 4 = CH_3COO^-, 5 = $C_6H_5COO^-$, 6 = L-Ala, 7 = L-Trp, 7' = D-Trp, 8 = L-Phe and 8' = D-trp)

2.3.2.3.1 Electrochemical studies of compound L^1H with various anions and amino acids

Interestingly, the window potential of $\mathbf{L^1H}$ system showed many peaks which are unusal behaviour of anthraquinone because of the effect of a carboxylic group in the $\mathbf{L^1H}$ as shown in Figure 2.12.[60, 78] Therefore, the cyclic voltammogram of $\mathbf{L^1H}$ was not similar to usual spectrum of anthraquinone. The first reduction possibly corresponded to the hydrogen bond interaction between carboxylic group and oxygen atom of anthraquinone before anthraquinone was reduced to be the semiquinone and dianion species, respectively.

This assumption was supported by literature evidences which suggested that stabilization of the reduced dianion in comparison to the semiquinone form as a result of intramolecular hydrogen bonding.[60] The shape of reduction wave indicated the CEE type mechanism. The following reaction sequence could be proposed : [31]

$$\mathbf{L^1H} + (RCOOH) \rightleftharpoons \mathbf{L^1H}(RCOOH) \quad (1)$$

$$\mathbf{L^1H}(RCOOH) \rightleftharpoons \mathbf{L^1H^-}(COOH) \quad (2)$$

$$\mathbf{L^1H^-}(COOH) + e^- \rightleftharpoons \mathbf{L^1H^{2-}}(COOH) \quad (3)$$

The electrochemical studies of $\mathbf{L^1H}$ and various anions and amino acids were not examined because the structure of $\mathbf{L^1H}$ was cleaved at NH_{imid}-C*H*-NH_{amid} of carboxylic side chain by strong bases.

2.3.2.3.2 Electrochemical studies of compound L^2H with various anions and amino acids

Complexations between ligand $\mathbf{L^2H}$ and various anions and amino acids were carried out in DMSO with Bu_4NPF_6 as supporting electrolyte. Figure 2.15 shows that the redox couple of $\mathbf{L^2H}$ species is similar to the literature report.[31] In the case of $\mathbf{L^2H}$, two consecutive one-electron quasireversible waves were observed, corresponding respectively to the formation of the semiquinone and dianionic intermediates (waves M and N) shown in Figure 2.12b.

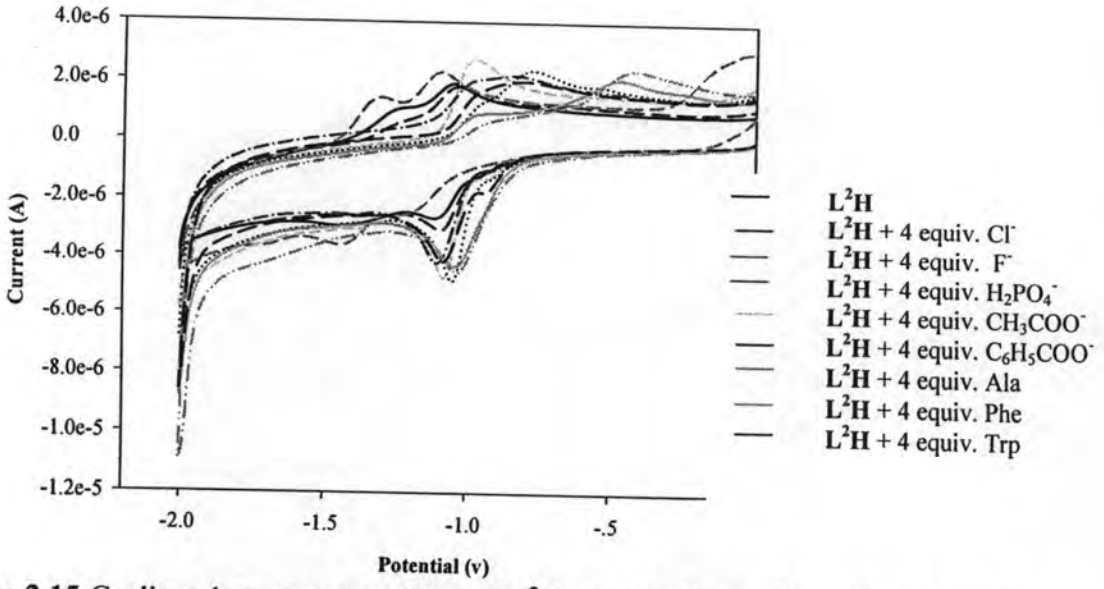

Figure 2.15 Cyclic voltammograms of ligand $\mathbf{L^2H}$ upon addition of 4 equiv. of various anions and amino acids.

The electrochemical studies of $\mathbf{L^2H}$ upon 4 equiv. of various anions and amino acids were shown in Figure 2.15 and the potential values were collected in Table 2.4. In the case of Cl^-, the cyclic voltammograms was slightly shifted from initial electrochemical potential because both anion can bind to ligand with a weak interaction. In the presence of CH_3COO^-, $C_6H_5COO^-$ and $H_2PO_4^-$, the Cyclic voltammograms displayed the enhancement semiquinone species observed by increasing intensity. Additionally, Cyclic voltammograms of these anions with $\mathbf{L^2H}$ showed a similar shape but gave the different shifts of reduction wave which depended on the basicity of anions.

Considering the Cyclic voltammograms of $\mathbf{L^2H}$ with 4 equiv. CH_3COO^- in Figure 2.16a, the Cyclic voltammograms are dramatically changed with the appearances of one reduction wave and one oxidation wave. It means that carboxylate anion inhibits the separation between semiquinone and dianion species.

In the case of F^-, the both of redox couples of $\mathbf{L^2H}$ show the cathodic shifts because of the enhancement of negative charge by the deprotonation process on NH amide moiety. It was displayed wave M2 and N2 in Figure 2.16b. Therefore, it is difficult to reduce the anthaquinone of $\mathbf{L^2H}$. Cyclic voltammogram of $\mathbf{L^2H}$ in the presence of 4 equiv. of Trp, Ala and Phe showed the same behaviors. The cyclic voltammograms of these amino acids showed a single reduction peak (labeled M8 in Figure 2.16c) on the anodic shift and followed by two oxidation with one high intensity and one low intensity

(labeled O8 and P8 in Figure 2.16c). From data analysis, the ammonium unit of amino acids likes to bind semiquinone species and sequent to stabilize the negative charge on anthraquinone. The new peak at M8 is similar to M4 of CH_3COO^- due to hydrogen bonding between the semiquinone and the $-NH_3^+$group of Phe. Therefore, we can deduce mechanism between $\mathbf{L^2H}$ and amino acids shown in equation (4)-(6).[26, 31]

$$\mathbf{L^2H} + e^- \rightleftharpoons \mathbf{L^2H^{\cdot -}} \quad (4)$$

$$\mathbf{L^2H^{\cdot -}} + {}^+NH_3RCOO^- \rightleftharpoons \mathbf{L^2H^{\cdot -}} \subset {}^+NH_3RCOO^- \quad (5)$$

$$\mathbf{L^2H^{\cdot -}} \subset {}^+NH_3RCOO^- + e^- \rightleftharpoons \mathbf{L^2H}^{2-}{}^+NH_3RCOO^- \quad (6)$$

Moreover, the structure of complex was proposed in the Figure 2.17. All interactions were undergone by the hydrogen bonding and electrostatic force interaction between the C(2)*H*, N*H*-amide and positive charge on imidazole unit of $\mathbf{L^2H}$ with the carboxylate group of amino acids and electrostatic force between the ammonium group of amino acids and reduced species of anthraquinone shown in Figure 2.17. Considering the data in Table 2.4 and Figure 2.16c, the potential shifts between free receptor and the bound receptor at the waves M, O and P were shown that at the wave M is in order of Phe, Trp and Ala, at the wave O is in order of Trp, Phe and Ala and at the wave P is in order of Phe and Ala. This was indicated that amino acids were bound with $\mathbf{L^2H}$ using hydrogen bonding and electrostatic force. From the Cyclic voltammograms results of $\mathbf{L^2H}$ with amino acids were in trend of Phe>Ala>Trp by observing of the changing potential reduction.

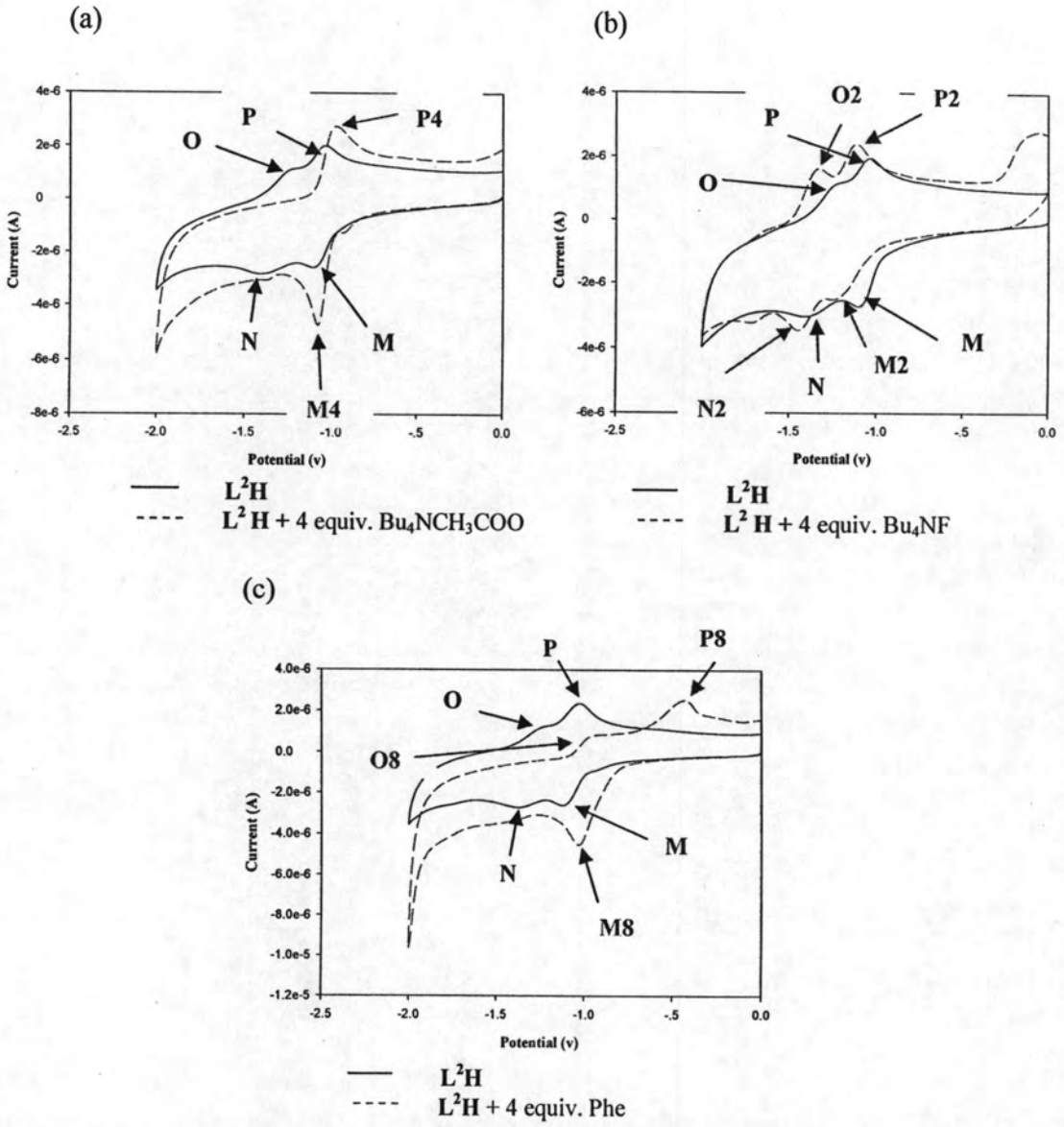

Figure 2.16 Cyclic voltammograms of ligand $\mathbf{L^1H}$ upon addition of 4 equiv. of a) Bu_4NCH_3COO, b) Bu_4NF and c) Phe

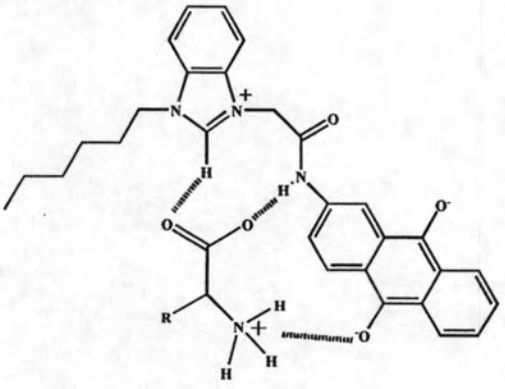

Figure 2.17 The propose structure of complex obtained by the reduced form of $\mathbf{L^2H}$ and zwitterionic amino acids.

2.3.2.3.3 Electrochemical studies of compound L^3H with various anions and amino acids

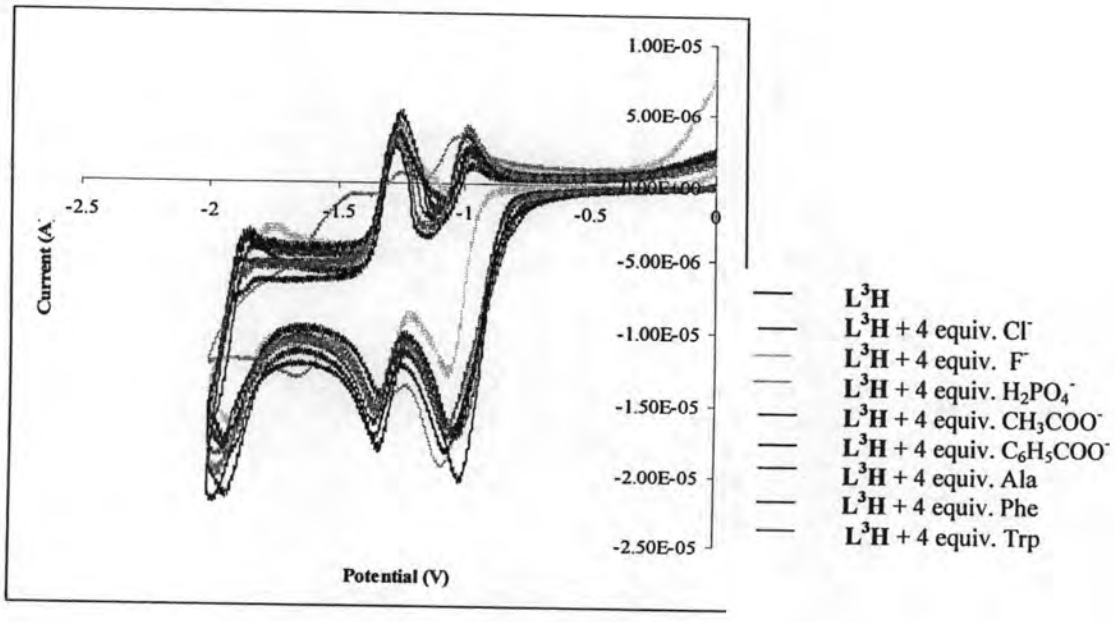

Figure 2.18 Cyclic voltammograms of ligand L^3H upon addition of 4 equiv. of various anions and amino acids

The L^3H was investigated on the complexation with various anions and amino acids showing the Cyclic voltammograms and the potential values in Figure 2.18 and Table 2.5. L^3H showed two one-electron irreversible, corresponding to the formation of semiquinone and dianonic species. The CV responses of L^3H with Cl^-, CH_3COO^-, $C_6H_5COO^-$, F^-, Ala and Phe changed slightly according to the reduction peak. The case of $H_2PO_4^-$ induced the significant change of cyclic voltammogram over other anions depicted in Figure 2.19a. Complexation between L^3H and $H_2PO_4^-$ was shown the 3 peaks of potential reduction. The first peak (wave W3) increases the intensity in the attribution of hydrogen bonding interaction of $H_2PO_4^-$ and anthraquinone. The second reduction peak shift to less negative potential at -1.304 V. Interestingly, there is the appearence of reduction peak at -1.624 V (wave S3). Importantly, L^3H has a selectivity for $H_2PO_4^-$ possibly caused by the suiTable geometry of $H_2PO_4^-$ for reduced form of L^3H which induces the strong hydrogen bonding interaction between both species in terms of the bond of P=O and P-O- towards NH-amide and C(2)H and P-OH towards –O- of dianion L^3H. The proposed structure of the complex between dianion L^3H and $H_2PO_4^-$ was exhibited in Figure 2.20.

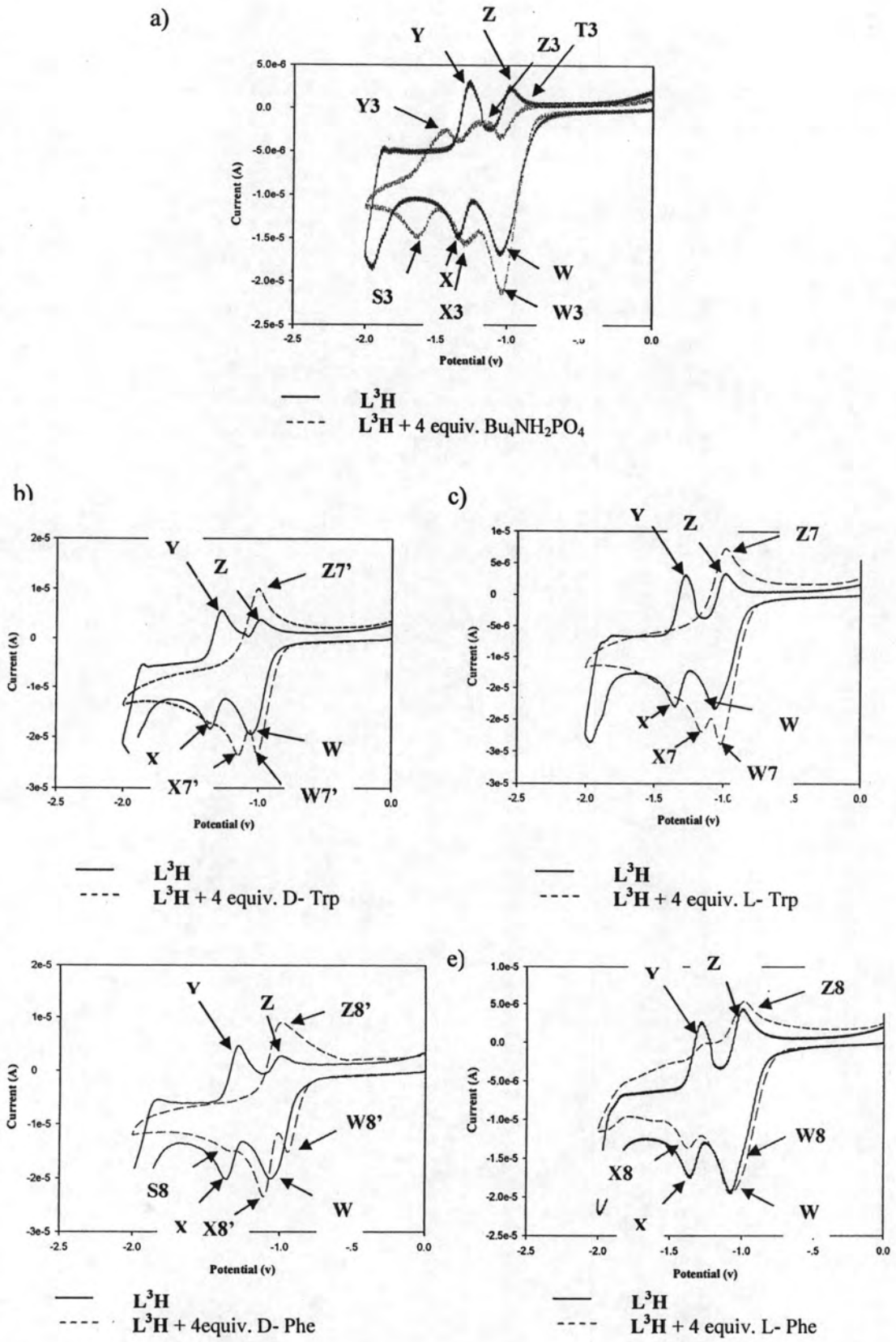

Figure 2.19 Cyclic voltammograms of ligand L^3H upon addition of 4 equiv. of a) $Bu_4NH_2PO_4$, b) D-Trp, c) L-Trp, d) D-Phe and e) L-Phe

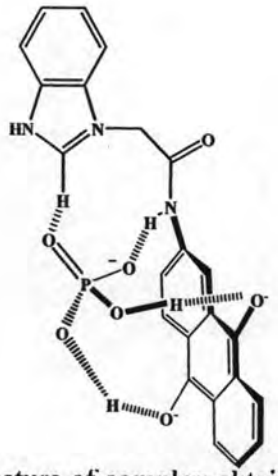

Figure 2.20 The propose structure of complex obtained by the reduced form of $\mathbf{L^3H}$ and $H_2PO_4^-$

In the presence of amino acids into $\mathbf{L^3H}$ solution, Ala was enable to slightly change the electrochemical potential reduction of $\mathbf{L^3H}$. For aromatic amion acids, Trp and Phe, the CV responds show the significant changes. Therefore, we would like to examine the enantioselectivity between L- and D- forms of amino acids. In the case of Trp, cyclic voltammogram showed two reduction peaks which shifted to less negative potential reduction. The first reduction (wave W7 and W7') showed the increased height due to the enhancement of the semiquinone species and the second reduction (wave X7 and X7') was shifted to less negative potential. Importantly, the anodic sweep was followed by an oxidation which increases the height (wave Z7 and Z7') at 0.991 V as shown in Figure 2.19b. It means that the hydrogen bonding would be occurred between the ammonium group of L-Trp and semiquinone. Since amino acids comprise of ammonium group which can stabilize reduced form of anthraquinone, $\mathbf{L^3H}$ is easy to be reduced and sequent to anodic shift. A similar CV response for $\mathbf{L^3H}$ and D-Trp was investigated. This means that $\mathbf{L^3H}$ could not differentiate between L- and D-Trp. Interestingly, CV response of $\mathbf{L^3H}$ with L- or D-Phe shows the different features. The reduction potential of $\mathbf{L^3H}$ with D-Phe, the first reduction was shown at -0.938V, the second and third reduction potentials were -1.106 and -1.360V, respectively. And following one oxidation was -0.994V. But the reduction potential of $\mathbf{L^3H}$ with D-phe, the first reduction was shown at -1.006V, the second potential was -1.162V and followed by an oxidation was -0.986V. Notably, $\mathbf{L^3H}$ is able to differentiate L- and D-Phe by cyclic voltammetric technique. These results were similar to in the case of $\mathbf{L^2H}$. Therefore, the mechanism of $\mathbf{L^3H}$ and Trp was deduced similarly to that of $\mathbf{L^2H}$ and amino acids as shown in equation (4)-(6).

From UV-vis technique, $\mathbf{L^3H}$ was not selective any anions and amino acids but for CV technique, $\mathbf{L^3H}$ seems to bind can respond to $H_2PO_4^-$ and Trp slectivity according to a large change of spectrum compound to other guests. Moreover, ammonium group of Trp showed the electrostatic force with semiquinone species in the cyclic voltammogramm.